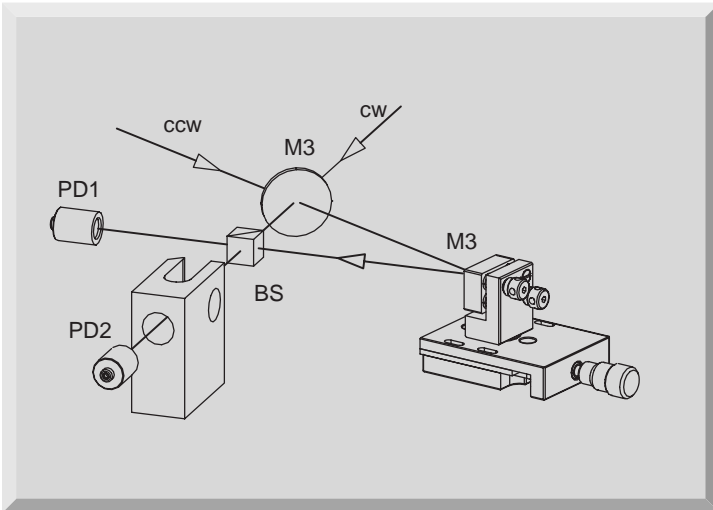
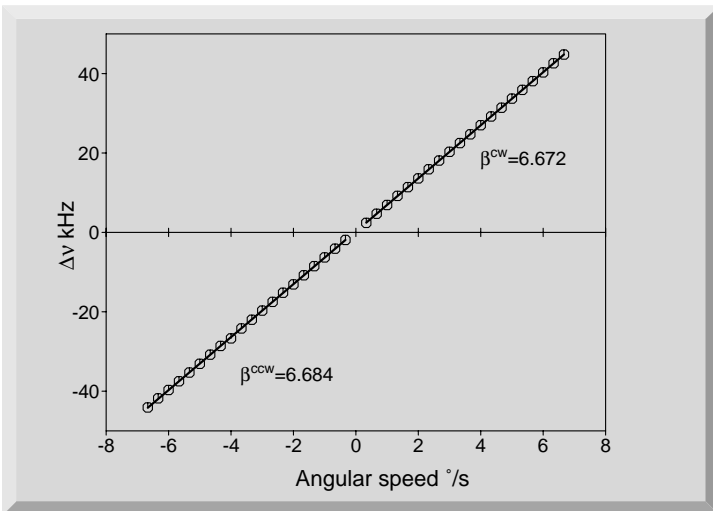


Experiment 16

Laser Gyro



Laserzentrum FH Münster
University of Appl. Sciences
Dept. Engineering Physics
- Prof. Dr. Klaus Dickmann -



1	INTRODUCTION	3
2	FUNDAMENTALS	3
2.1	Characteristics of light	3
2.2	Superimposition and Phase δ	6
2.3	Interferometer	7
2.4	Sagnac Effect	8
2.5	Ring Resonator	10
2.6	ABCD Matrices	11
2.7	Helium Neon Laser	13
2.7.1	He-Ne energy- level diagram	13
2.7.2	Gain Profile of Neon	14
2.8	Modes of the ring resonator	16
2.9	Mode selection	17
2.10	Transverse modes	18
2.11	The Laser gyro	19
2.11.1	Lock-in Effect	20
2.12	Measuring of the beat frequency	21
2.12.1	Interference	21
2.12.2	Beam analysis	22
3	EXPERIMENTS	23
3.1	Description of the Components	25
3.1.1	First adjustment Step 1	28
3.1.2	Initial adjustment step 2	28
3.1.3	Initial adjustment step 3	29
3.1.4	Initial adjustment step 4	29
3.1.5	Adjusting the interference optics	30
3.2	Rotation drive of the Laser Gyro	31
3.3	Measurements	32
3.3.1	Instrument scale factor	32
3.3.2	Measuring the Lock-in threshold	32
3.3.3	Angle measurement	33
4	APPENDIX	34
4.1	Measuring table for the determination of the scale factor	34
4.2	Measuring table for the determination of the Lock-in threshold	34

1 Introduction

Navigation is one of the oldest arts known to man and comprises of reaching a destination starting from a source by taking the shortest possible route. In very rare cases is this shortest route a straight line, obstacles have to be overcome so that in general, the route represents straight pieces placed one after the other. The job of the navigator hence, is to keep the deviation from the planned course as low as possible and that too, during both the day and night. For this purpose, he must have an instrument that shows him the direction of the planned course and he must know the distance that has already been covered. The oldest instrument providing information about the direction is the magnetic compass, which was already being used by the Chinese in 200 – 300 BC. The compass came to the west only in the 14th century AD. The Chinese already knew about the wrong indications of the compass and one tried to discover instruments that are more suitable. In 1878, Foucault could demonstrate with the help of a gyroscope, that a hanging rotating mass tries to retain its impulse axis in space. The wars around 1910 led to the development of a gyrocompass, the kind of which is being used nowadays in sea navigation. In 1913, Sagnac developed an apparatus that could determine the changes in the angular speed through optical interference. However, no one at that time gave a serious thought to use this as a substitute for the gyrocompass. This situation changed after the discovery of the Laser in 1960. The advantage of a laser gyroscope is undoubtedly the fact that such systems do not contain any rotating mass, and hence are insensitive to linear accelerations as compared to the mechanical gyroscopes. Especially noteworthy is also the higher measurement range of $0.01 \text{ }^\circ/\text{h}$ to $1000 \text{ }^\circ/\text{s}$, so that these systems can also be used in fast flying objects. Today, Laser gyroscopes are being used in commercial aircrafts like the Airbus or in carrier rockets like the Ariane.

The aim of this project is the introduction and the testing of a Helium Neon ring laser gyroscope. Certain fundamental concepts have been explained below to ensure a better understanding of such a system.

2 Fundamentals

2.1 Characteristics of light

Light, the giver of life, has always held a great fascination for human beings. It is therefore no coincidence that people have been trying to find out what light actually is. We can see it, feel its warmth on our skin, but we cannot touch it. The ancient Greek philosophers thought light was an extremely fine kind of dust, originating in a source and covering the bodies it reached. They were convinced that light was made up of particles. As humankind progressed and we began to understand waves and radiation, it was proved that light did not, in fact, consist of particles but that it is an electromagnetic radiation with the same characteristics as radio waves. The only difference is in the wavelength. We now know that the characteristics of light are revealed to the observer depending on how he sets up his experiment. If the ex-

perimenter sets up a demonstration apparatus for particles, he will be able to determine the characteristics of light particles. If the apparatus is one used to show the characteristics of wavelengths, he will see light as a wave. The question we would like to be answered is: What is light in actual fact? The duality of light could only be understood using modern quantum mechanics. Heisenberg showed, with his famous “uncertainty relation”, that strictly speaking, it is not possible to determine the place x and the impulse p of any given occurrence at the same time

$$\Delta x \cdot \Delta p_x \geq \frac{1}{2} \hbar$$

If, for example, the experimenter chooses a set up to examine particle characteristics, he will have chosen a very small uncertainty of the impulse p_x . The uncertainty x will therefore have to be very large and no information will be given on the course of the occurrence. Uncertainties are not given by the measuring apparatus, but are of a basic nature. This means that light always has the particular quality the experimenter wants to measure. We can find out about any characteristic of light as soon as we think of it. Fortunately, the results are the same, whether we work with particles or wavelengths, thanks to Einstein and his famous formula:

$$E = m \cdot c^2 = \hbar \cdot \omega$$

This equation states that the product of the mass m of a particle with the square of its speed c corresponds to its energy E .

It also corresponds to the product of Planck’s constant $\hbar = \hbar \cdot 2\pi$ and its radian frequency $\omega = 2\pi \cdot \nu$. In this case ν represents the frequency of luminous radiation. In our further observations of the fundamentals of the Michelson interferometer, we will use the wave representation and describe light as electromagnetic radiation. All types of this radiation, whether in the form of radio waves, X-ray waves or light waves consist of a combination of an electrical field \vec{E} and a magnetic field \vec{H} . Both fields are bound together and are indivisible. Maxwell formulated this observation in one of his four equations, which describe electromagnetic fields

$$\nabla \times \vec{H} \approx \frac{\partial \vec{E}}{\partial t}$$

According to this equation, every temporal change in an electrical field is connected to a magnetic field (Fig.1).

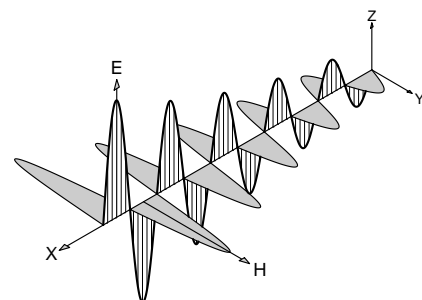


Fig. 1: Light as electromagnetic radiation

Due to the symmetry of this equation, a physical condition can be sufficiently described using either the electrical or the magnetic field. A description using the electrical field is preferred since the corresponding magnetic field can then be obtained by temporal derivation. In the experiments (as presented here) where light is used as electromagnetic radiation, it is advantageous to calculate only the electrical fields since the light intensity is:

$$I = \frac{c \cdot \epsilon}{4\pi} \cdot |\vec{E}|^2.$$

This is also the measurable size as perceived by the eye or by a detector. In this case, the speed of light is c in the respective medium and ϵ is the corresponding dielectrically constant. Since we are comparing intensities in the same medium, it is sufficient to use

$$I = |\vec{E}|^2$$

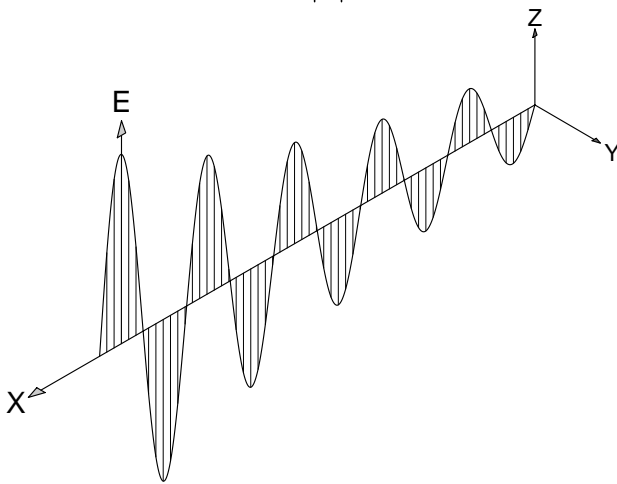


Fig. 2: In this experiment we need only to observe the electrical field strength E

The experimental findings agree with the theory of electromagnetic radiation if a harmonic periodic function becomes temporally dependent on the field strength of light. In its simplest form, this is a sine or cosine function. An amplitude E_0 and a wavelength λ should be used in the definition of this kind of function. Let us begin with the equation:

$$E_x = E_0 \cdot \sin\left(\frac{2 \cdot \pi}{\lambda} \cdot x\right), \quad (1)$$

which we will elaborate and explain further.

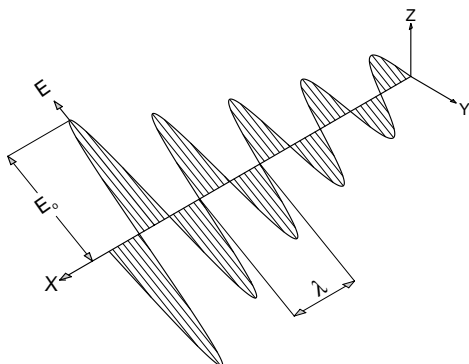


Fig. 3: Amplitude and wavelength

In the above figure, the light wave no longer oscillates in the Z-direction as in Fig.2 but at a certain angle to the Z- or Y-axis. The X-axis has been chosen as the direction of propagation of the wave. We still require information on the direction in which the electrical field strength E_x oscillates to complete the description of the wave. Strictly speaking, the field E_x oscillates vertically to the direction of propagation X. However, we have to give information regarding the Z- and Y-axis. This leads to the term 'Polarisation' and Direction of Polarisation. In Figs. 1 and 2 we used linearly polarised light with a polarisation direction in Z and in Fig.3 we used a different direction. We will now introduce the polarisation vector P, which is defined in the following Fig.4. We have to look into the light wave in the direction of the X-axis for this purpose.

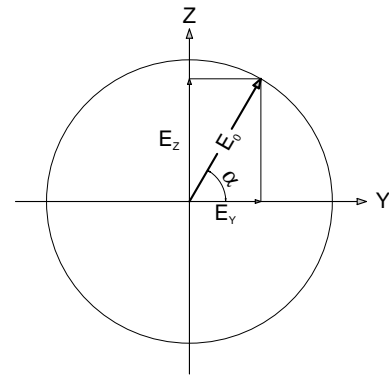


Fig. 4: Definition of the polarisation vector

We can observe a wave expanding in the X-direction and oscillating at the electrical field amplitude E_0 below an angle α to the Y-axis. The amplitude E_0 is separated into its components, which oscillate in the Z- or Y-direction. We now write \hat{E}_0 instead of E_0 to indicate that the amplitude E_0 is now made up of individual components.

$$\hat{E}_0^2 = (E_0^Y)^2 + (E_0^Z)^2 = (E_0^Y \cdot \hat{e}_Y + E_0^Z \cdot \hat{e}_Z)^2$$

In this case $\hat{e}_Z = (0,1)$, $\hat{e}_Y = (1,0)$ is the unit vector in the Z- or Y-direction on the ZY-plane. Characteristically the unit vectors yield $|\hat{e}_Z|=1$ and the scalar product $\hat{e}_Z \cdot \hat{e}_Y = 0$. The equation (1) can now be generalised to:

$$E_x(Y,Z) = (E_0^Y \cdot \hat{e}_Y + E_0^Z \cdot \hat{e}_Z) \cdot \sin\left(\frac{2\pi}{\lambda} \cdot x\right)$$

At this point, we come across a fundamental principle in classic wave theory, i.e. the principle of superimposition. A big word for the simple statement:

Every wave can be represented as the sum of individual waves.

In our example we had separated the wave as shown in Fig.4 into two individual waves, i.e. one that oscillates in the Z-direction and another in the Y-direction. We could just as well say that our wave was formed by the superimposition of these two individual waves. The word *interference* can also be used to mean superimposition. In this context, our wave was formed by the interference of two individual waves. This is the basis for the function-

ing of the Michelson interferometer. An introduction to this interferometer now follows. For the time being, let us return to the polarisation vector.

The polarisation vector \hat{P} is also a unit vector, which always points in the direction of the oscillation of the electrical field E_x

$$\hat{P} = \frac{\hat{E}_0}{|\hat{E}_0|} = \frac{E_0^Y}{E_0} \cdot \hat{e}_Y + \frac{E_0^Z}{E_0} \cdot \hat{e}_Z,$$

or as is written for vectors

$$\hat{P} = \left(\frac{E_0^Y}{E_0}, \frac{E_0^Z}{E_0} \right).$$

The polarisation vector for a polarisation in the Z-direction (0°) would then be, for example:

$$\hat{P} = (0, 1)$$

for a polarisation direction of 45° it would be:

$$\hat{P} = \frac{1}{\sqrt{2}}(1, 1).$$

The equation of the wave with any given polarisation direction will thus be

$$\hat{E}_x(Y, Z) = \hat{P} \cdot E_0 \cdot \sin\left(\frac{2\pi}{\lambda} \cdot x\right), \text{ or}$$

$$\hat{E}_x(Y, Z) = (E_Y, E_Z) \cdot \sin(k \cdot x). \quad (2)$$

We have introduced the wave number k in the above equation

$$k = \frac{2\pi}{\lambda}.$$

The wave number k has the length dimension⁻¹ and was originally introduced by spectroscopists because it was a size that could be measured immediately with their equipment. We are using this size because it simplifies the written work.

Till now we have only described the wave as a function of the location. This would be sufficient in order to understand the classical Michelson interferometer, but not for technical interferometers. We carry out the following hypothetical experiment to introduce the "time coordinate":

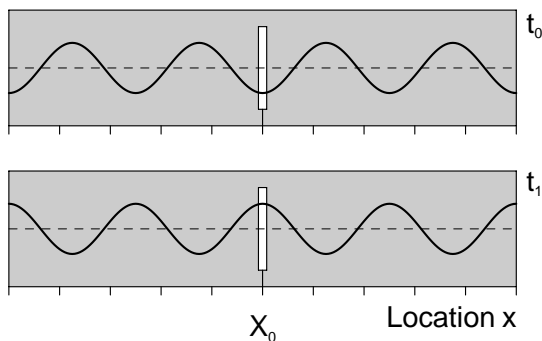


Fig. 5: Hypothetical experiment for the introduction of dependency on time

The talented physicist Walter S. * (*Names have been changed) is working on new experiments with electro-

magnetic waves in his laboratory. His colleague Gerd N. who is jealous of his rival's success sees that the door to Walter S.' laboratory has been left open a crack and uses the opportunity to find out what his colleague is working on. In spite of his nervousness, Gerd N. forces himself to make painstakingly accurate notes of his observations. He measures the time with his Swiss stop watch, a present from his father, who was also a physicist and notes the respective intensities of what he sees through the crack in the door. He rushes into his modest study, red in the face, and writes his observations into his laboratory records. Here we find the following entries:

".....I stood at location X and looked through the crack in the door. I observed periodic oscillations in field strength, which fluctuated between a maximum and a minimum. I began measuring at the time $t=0$, when the field strength was at its minimum. At the time t_1 I calculated the maximum field strength. The differences in time between the extreme values stayed constant." A graph of his measurement values follows:

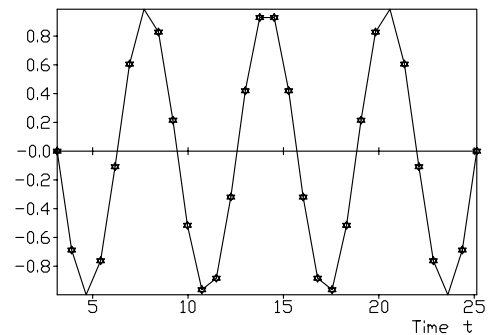


Fig. 6: Gerd N's measurement curve

Gerd N. further states that: "..... the time that passed between two maxima as the duration period τ . I have observed n of such maxima within one second. Obviously,

the field strength has a frequency of $\nu = \frac{n}{\tau}$ and follows

a periodic function $E = E_0 \cdot \sin(2\pi \cdot \nu \cdot t)$ although this function begins with positive values. The measured values only correspond to the observations if a constant is added to the argument of the sine

$$E = E_0 \cdot \sin\left(2\pi \cdot \nu \cdot (t - t_0)\right).$$

Some weeks later both colleagues meet at a specialists' conference. As is often the case, the evening session of the conference took place in a suitable atmosphere, where the participants committed themselves to the team spirit over a glass of wine and agreed on all other things as well. Walter S. spoke openly about how he had managed to formulate the position of the course of a wave and wrote his formula on the beer mat, commonly used in this area

$$E = E_0 \cdot \sin\left(\frac{2\pi}{\lambda} \cdot (x - x_0)\right).$$

How the evening finally ended is left to your own imagination. What is important is that both experimentalists measured the same field strength, one with a stopwatch in his hand, the other with a scale. Therefore

$$\frac{E}{E_0} = \sin(2\pi \cdot v \cdot (t - t_0)) = \sin\left(\frac{2\pi}{\lambda} \cdot (x - x_0)\right).$$

This is the same as

$$v \cdot (t - t_0) = \frac{1}{\lambda} \cdot (x - x_0)$$

or

$$v \cdot \lambda = \frac{(x - x_0)}{(t - t_0)} = c.$$

This hypothetical experiment has shown us that we can describe the wave by its temporal course on the one hand, and by the position of the course of a wave on the other. We have also found out the importance of the relationship of the speed c of a wave to its frequency and wavelength $v = \frac{c}{\lambda}$.

If we write the connection with $\omega = 2\pi v$ as a rotary frequency we get:

$$\omega = \frac{2\pi}{\lambda} \cdot c = k \cdot c.$$

Let us now return to the generalised formula for the temporal and spatial course of the field strength of a light wave. Since the sine is a periodic function, we can include the temporal and spatial dependency into the argument. We would then get

$$\hat{E}_x(Y, Z) = (E_Y, E_Z) \cdot \sin(k \cdot (x - x_0) + \omega \cdot (t - t_0))$$

If we now make the constants kx_0 and ωt_0 into one constant δ we obtain the general formula

$$\hat{E}_x(Y, Z) = (E_Y, E_Z) \cdot \sin(k \cdot x + \omega \cdot t + \delta) \quad (3)$$

2.2 Superimposition and Phase δ

δ is also described as a phase. Since this term is often inconvenient, we would like to examine it more closely. If we put $x=0$ and $t=0$ into (3) the field strength will have a value of $\hat{E}_x(Y, Z) = (E_Y, E_Z) \cdot \sin(\delta)$ and thus defines an initial value for the amplitude. This value is or will be determined according to the physical situation.

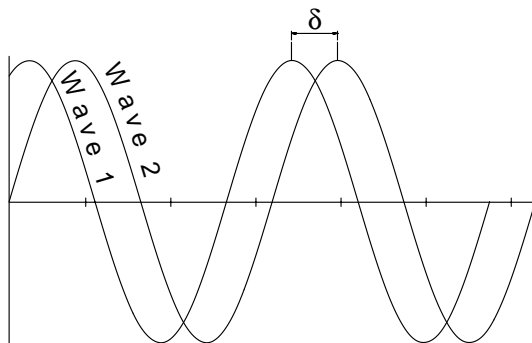


Fig. 7: Definition of phase δ

Obviously, phase δ contains information about the relationship between two or more waves. Let us presume that the waves originate in a light source and phase δ contains information on how the wave was formed. Light waves are formed by emission processes. There is an emission procedure for every photon or light wave. Such processes are always taking place when the light source is continuously illuminated. The emission procedures are distributed statistically according to the type of light source. Thus, phase δ is also distributed statistically. If the emission procedures are coupled to each other, as is the case with lasers, and all photons or waves have the same frequency or wavelength (they are monochromatic) the light is then described as coherent (holding itself together). If, however, phase δ is randomly distributed, then this light is incoherent. This is the case with thermal light sources, e.g. light bulbs. To judge the coherence of a light source, the characteristics of the emitted waves and/or photons would have to be classified. The waves (photons) are first sorted out according to their frequencies (wavelengths) and then according to their phases. If we form small “containers” in our minds with the labels:

$$k = \frac{2\pi}{\lambda} = \text{numerical value and}$$

$$\delta = \text{numerical value}$$

and if we now sort out the photons in these containers and then count the photons per container, we could obtain a statement on the coherence. This kind of container is also called a phase cell. If all photons were in one container or phase cell, the light would be completely coherent.

In the example according to Fig.7, the wave 2 has a phase of δ as opposed to the wave 1; in other words, the waves have a phase difference of δ , presuming that we have produced two such waves (this is exactly what the Michelson interferometer does). We expect a third wave through the principle of superimposition, which is formed by the superimposition or interference of the two basic waves. We will find out how this wave looks by simply adding both basic waves:

$$\text{Wave 1 } \hat{E}_1(Y, Z) = (E_Y, E_Z) \cdot \sin(k \cdot x + \omega \cdot t + \delta)$$

$$\text{Wave 2 } \hat{E}_2(Y, Z) = (E_Y, E_Z) \cdot \sin(k \cdot x + \omega \cdot t)$$

$$\text{Wave 3 } \hat{E}_3(Y, Z) = \hat{E}_1(Y, Z) + \hat{E}_2(Y, Z)$$

It is now easy to imagine that a large number of waves with different frequencies ω or wavelengths λ and phases δ result in such a mixture and that it makes little sense to carry out superimposition or interference experiments with this light. Therefore light sources which emit light within a narrow emission spectrum with a phase as constant as possible are selected. Lasers are an example of such light sources. However, when Michelson carried out his experiments around 1870 he could not use lasers. He used the red emission line of a cadmium lamp whose emission bandwidth showed a coherence length of only 20 cm. This means that when, for example, waves at the position $x=0$ were superimposed with those at the position $x=20$, there was no readable interference any more.

We will come back to the important term “*coherence length*” later on and discuss it in more detail.

2.3 Interferometer

An apparatus that produces this physical condition is shown in the following diagram.

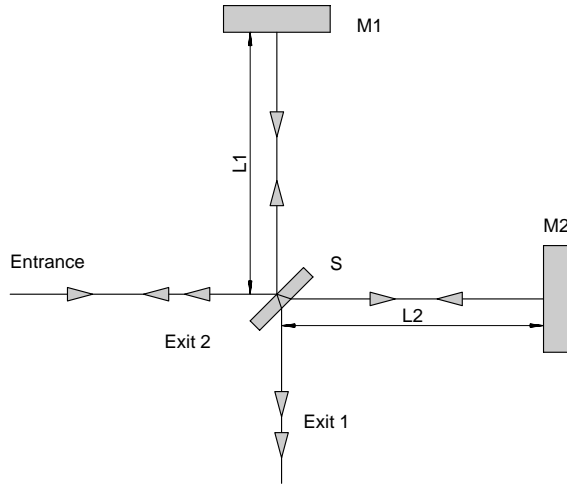


Fig. 8: Michelson interferometer.

We beam light into the entrance of the interferometer from some light source. The light is split into two bundles on a beam-splitting plate S. One bundle hits the mirror M1 and the other the mirror M2. The bundles will reflect back in themselves at these mirrors and reunite at the beam-splitting plate S. The respective bundles are split into two further bundles due to the characteristics of the beam-splitting plate and one bundle is led in the direction of exit 1, the other in the direction of exit 2 in the process. Exit 2 of the Michelson interferometer points in the direction of the light source, so this exit is practically of no use to us to set up photodetectors or imaging screens. This is why only exit 1 will be mentioned. However, exit 2 must also be taken into consideration for the energy balance. Whatever technical model of an interferometer is chosen, it can be represented easily in an optically circuit diagram.

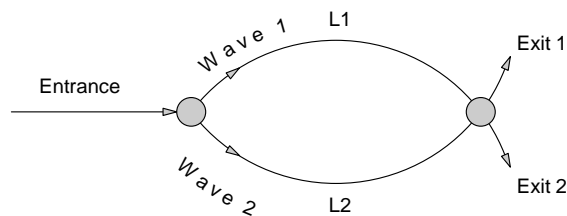


Fig. 9: "Optical circuit diagram" of an interferometer

The light, which is put into the entrance of the interferometer, is split into two bundles. How this happens technically is not important for the time being. This kind of element can generally be called a directional coupler. Bundle 1, or, in the simplest case, the wave 1 runs through the path L1 and the other wave 2 runs through the path L2. Both waves are brought together in a mixer. This mixer has two exits. In the Michelson interferometer, directional couplers and mixers are the same ele-

ment. We are only interested in exit 1 for the time being. As we will see later on, exit 2 is symmetrical to exit 1. We now just have to calculate wave 3 at exit 1 which is formed out of the superimposition of wave 1 with wave 2 which have travelled along a path from L1 or L2. Without jeopardizing the general validity of the solution, we can assume that the electric field strength only oscillates in the Y-direction. As already defined in the beginning the waves propagate in the X-direction. Although the direction of the bundle of rays can point in other directions after separation, they should have the same direction of propagation, at least in the mixer, if they are to interfere at all.

$$\text{Wave 1} \quad E_1 = E_{01} \cdot \sin(k \cdot L_1 + \omega \cdot t)$$

$$\text{Wave 2} \quad E_2 = E_{02} \cdot \sin(k \cdot L_2 + \omega \cdot t)$$

$$\text{Wave 3} \quad E_3 = E_1 + E_2$$

Since both waves, E_1 and E_2 are formed when the entering wave E_0 is split and the splitter should separate them symmetrically, both partial waves do not have any phase shift δ with regard to each other.

$$E_3 = E_{01} \cdot \sin(k \cdot L_1 + \omega \cdot t) + E_{02} \cdot \sin(k \cdot L_2 + \omega \cdot t)$$

A screen or photodetector is installed at exit 1. The human eye and the photodetector are not in a position to register electric field intensities, but can only register the light intensity I which is connected to the field strength:

$$I = E^2$$

$$I = (E_{01} \cdot \sin(k \cdot L_1 + \omega \cdot t) + E_{02} \cdot \sin(k \cdot L_2 + \omega \cdot t))^2$$

$$I = E_{01}^2 \cdot \sin^2(kL_1 + \omega t) + 2E_{01}E_{02} \sin(kL_1 + \omega t) \sin(kL_2 + \omega t) + E_{02}^2 \cdot \sin^2(kL_2 + \omega t)$$

To simplify the mixed term we use the relation:

$$2 \cdot \sin \alpha \cdot \sin \beta = \cos(\alpha - \beta) + \cos(\alpha + \beta)$$

and obtain:

$$I = E_{01}^2 \cdot \sin^2(kL_1 + \omega t) + E_{01}E_{02} \cos(k(L_1 - L_2)) + E_{01}E_{02} \cos(k(L_1 + L_2) + 2\omega t) + E_{02}^2 \cdot \sin^2(kL_2 + \omega t)$$

The expression for light intensity, which is perceived either by a detector or by our own eyes, consists of four terms. Only the second term is not dependent on the time

t. All other terms oscillate with the frequency ω . We use

$$\omega = 2\pi\nu = 2\pi \frac{c}{\lambda}$$

to determine this ω . The frequency of light is ν and has a wavelength λ and a speed c . In the later experiments, we will select the light emitted by a Helium-Neon laser. The wavelength of this light is 633nm. Using this value and the speed of light $c = 3 \cdot 10^8$ m/s the frequency ν is calculated as:

$$\nu = \frac{3 \cdot 10^8}{633 \cdot 10^{-9}} = 4,7 \cdot 10^{14} \text{ Hz.}$$

The sine of the first and last term oscillates at this frequency and the third even oscillates at double this frequency. Neither the eye nor any photodetector is capable of following this extremely high frequency. The fastest photodetectors nowadays can follow frequencies of up to approx. $2 \cdot 10^9$ Hz. This is why a detector, and even more so, our eyes can only perceive average values. The \sin^2 terms oscillate between 0 and 1; their temporal average value is therefore 1/2. The cosine term oscillates between -1 and +1 and the average value is zero. The intensity I would therefore be:

$$I = \frac{1}{2} E_{01}^2 + \frac{1}{2} E_{02}^2 + E_{01} E_{02} \cos(k \cdot \Delta L)$$

$$\Delta L = L_1 - L_2.$$

Obviously, I is maximum if the cosine is one. This is always the case when its argument is zero or an integral multiple of 2π . I is minimum just at the time when the cosine is -1

$$I_{\max} = \frac{1}{2} E_{01}^2 + \frac{1}{2} E_{02}^2 + E_{01} E_{02} = \frac{1}{2} (E_{01} + E_{02})^2$$

$$I_{\min} = \frac{1}{2} E_{01}^2 + \frac{1}{2} E_{02}^2 - E_{01} E_{02} = \frac{1}{2} (E_{01} - E_{02})^2$$

Let us remind ourselves that

$$k = \frac{2\pi}{\lambda}$$

and that it is constant at a stable wavelength. The light intensity at exit 1 is therefore obviously only dependent on the path difference $L1-L2$. If both paths having the same length, both partial waves interfere constructively and the light intensity observed is maximum. If the path difference is just $\lambda / 2$ then:

$$k \cdot \Delta L = \frac{2\pi}{\lambda} \cdot \frac{\lambda}{2} = \pi.$$

The cosine is then -1 and the light intensity I at the exit becomes minimum. Let us divide the initial intensity into two partial ones of equal size, i.e. E_{01} and E_{02} . In this case, even the light intensity is zero. Here, both partial waves interfere destructively. Keeping in mind that the wavelength for our experiment is 633 nm and that it leads to a shift from one wave to another by only

$\lambda/2=316.5 \text{ nm} = 0.000000316 \text{ mm}$ (!) from a light to a dark transition at exit 1, this type of interferometer is a highly precise apparatus for measuring length.

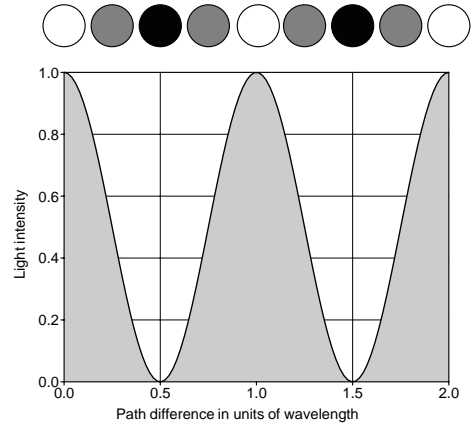


Fig. 10: Interferogram

With the knowledge of the preceding chapters, we are now prepared to approach the main topic of this project, the laser gyroscope.

2.4 Sagnac Effect

Whereas the Michelson interferometer is mostly suitable for measuring translations, there are also certain special arrangements, with the help of which one can measure rotations with a very high degree of accuracy. The starting point of the research, however, was not based on technical applications, but instead served to test the theory of relativity of Einstein from 1910 - 1920. During that time, the relativity principle of electrodynamics referred exclusively to translation movements. However, it was already known from Mechanics, that natural processes behave differently in a rotating system than in a non-rotating system. This is shown, for example, by the pendulum experiment of Foucault, which has proven the rotation of Earth. The equations of motion of rotating mechanical systems were changed as a result to the extent that apparent forces like the centrifugal and the Coriolis force were integrated. Harress (1912) and then Sagnac (1913) studied the question of how electromagnetic radiation like light would behave in a rotating system. We shall discuss here first the results of Sagnac, since the laser gyroscope was based on them.

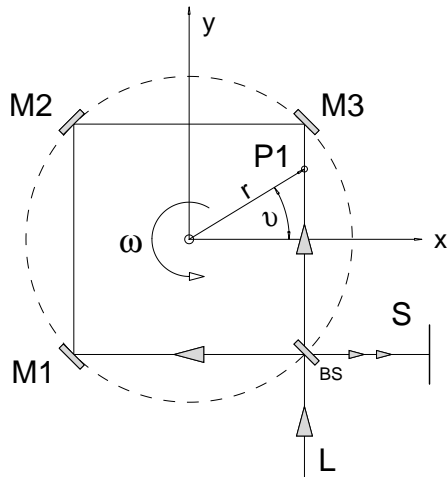


Fig. 11: Sagnac Interferometer

In this experiment the light from the source L is split by the beam splitter BS in such a way, that one half of the intensity goes in the clockwise direction and the other in the counter-clockwise direction, reflected by the mirrors M1 to M3, and then again leave the beam splitter together. The interference pattern is recorded on the screen S. The complete arrangement including the light source, mirrors, screen and the observer are placed on a rotatable platform, whose centre of rotation is in the centre of the interferometer. At rest, an interference pattern is observed on the screen, which however, changes when the whole arrangement starts rotating. Apparently, the rotation causes a phase difference to occur between the two waves. We shall now calculate this phase difference. For this we assume that the platform is rotating in counter-clockwise direction with an angular speed of ω . The task is first to determine the velocity v for all the elements ds of the path of the light rays and then to determine their run-time difference ΔT .

$$\Delta T = T_- - T_+ = \oint \frac{ds}{v_-(ds)} - \oint \frac{ds}{v_+(ds)} \quad (4)$$

The number N of the continuous bright- dark-transitions is calculated in the same way as in Michelson interferometer:

$$N = \Delta T \cdot \nu = \Delta T \cdot \frac{c}{\lambda} \quad (5)$$

Whereby c is the speed, ν the frequency and λ the wavelength of the light rays used. We shall now go on to determine equation (4).

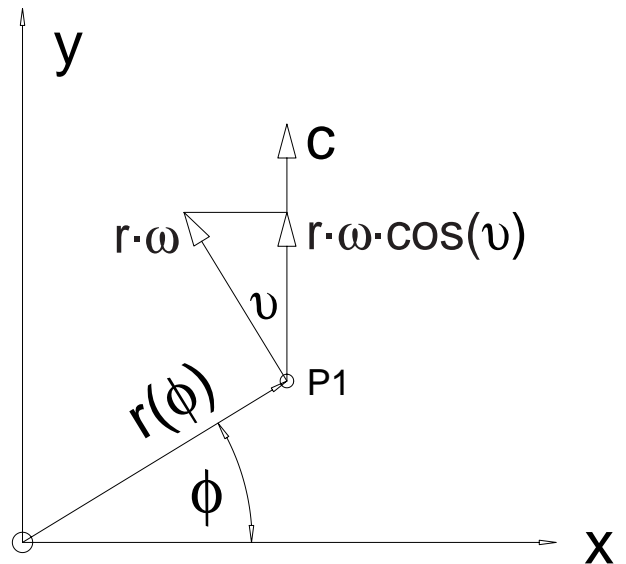


Fig. 12: Speed components analysis

We shall first consider the speed of the wave, which spreads out from the point P1 in the direction of rotation v_+ . The linear velocity v here, at a distance r from the centre of rotation, is:

$$v = r \cdot \omega$$

However, for the linear element ds in the direction of the wave, it is:

$$v = r \cdot \omega \cdot \cos \nu$$

This gives the total speed of the wave for the linear section ds as:

$$v_+ = c + r \cdot \omega \cdot \cos \nu$$

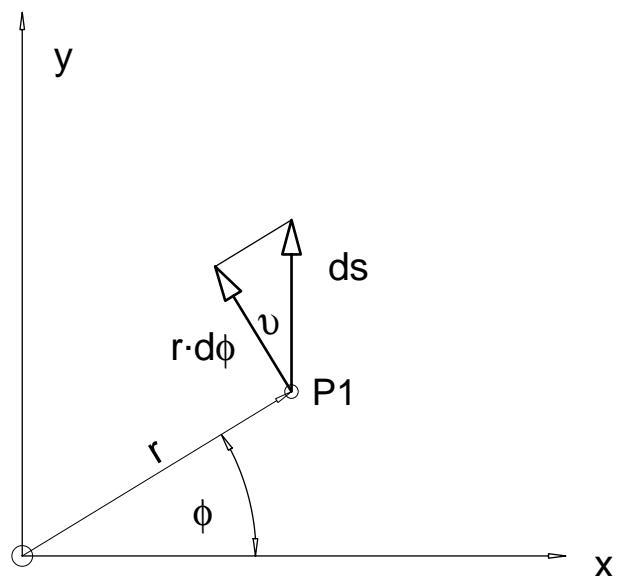


Fig. 13: Determining cos (ν)

From figure 13, we can see the following context:

$$\cos \nu = \frac{r \cdot d\phi}{ds}$$

The equation (4) thus becomes:

$$\Delta T = \oint \frac{ds}{c - r^2 \cdot \omega \frac{d\phi}{ds}} - \oint \frac{ds}{c + r^2 \cdot \omega \frac{d\phi}{ds}}$$

Or

$$\Delta T = \frac{2\omega}{c^2} \oint \frac{r^2 d\phi}{1 - \left(r^2 \cdot \frac{\omega}{c} \cdot \frac{d\phi}{ds}\right)^2}$$

since $\frac{\omega}{c} \ll 1$ the above equation gets simplified to:

$$\Delta T = \frac{2\omega}{c^2} \oint r^2 d\phi = \frac{4F}{c^2} \cdot \omega,$$

whereby F denotes the encompassed area. From equation (5) we get the following for the number of bright- dark transitions (fringes):

$N = \frac{4F}{c\lambda} \cdot \omega$	(6)
--	-----

The number of fringes is thus proportional to the angular speed ω and the area F, which is surrounded by the path of the light rays. This displacement of the interference pattern by N fringes is also actually observed. In one of his experiments, Sagnac used a fast rotating disc with a diameter of 1 m. In other experiments he used a much bigger light path on board a ship, whereby the angular speed was achieved by driving around narrow curves. Similarly, Michelson and Gale (1925) had used the rotation of Earth itself to verify the effect. Here he is supposed to have used a light path of many kilometres and still been able to prove the relatively small value of ω of the rotation of Earth. These can be considered as some excellent achievements of engineering if one considers the conditions at that time, when such a coherent source of light as a laser was still not available. Even Einstein was awed by the achievement of Michelson and Gale, who with the help of his ingenious construction, were able to prove the rotation of Earth and did not become a victim of mirror adjustments or other dirt effects. About 70 years after the works of Michelson, scientists at the University of Canterbury again constructed an interferometer, to measure the rotation of Earth. The so-called CII Interferometer, which is now equipped with a laser and has been made out of a Zerodur block to ensure a long-term stability. This has been placed in a bunker in the Cashmere Cavern (New Zealand). Together with many institutions, the questions about the constancy of the rotation of earth and the theory of relativity are being worked out here. In the next section we shall learn about

the structure of the interferometers being used nowadays that use the Sagnac effect for measuring rotations.

2.5 Ring Resonator

The interferometers used by Sagnac were characterized by the fact, that the light source was present outside the resonator. In the laser gyroscopes of today, there is an arrangement, in which the light source is present within the interferometer. The mirrors of the interferometer also function at the same time as resonator mirrors of a laser. In more exact words, the arrangement can be described as a ring laser. The arrangements, as given in fig. 14, are very familiar.

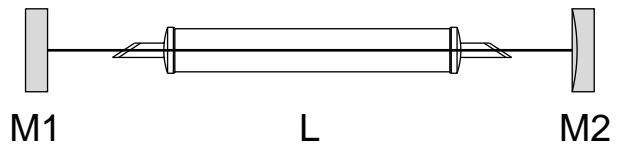


Fig. 14: Two-mirror laser

However, the structure can be expanded by two more mirrors to get a ring laser, in which no standing waves are generated as in the two-mirror resonator, but instead, gyrating waves.

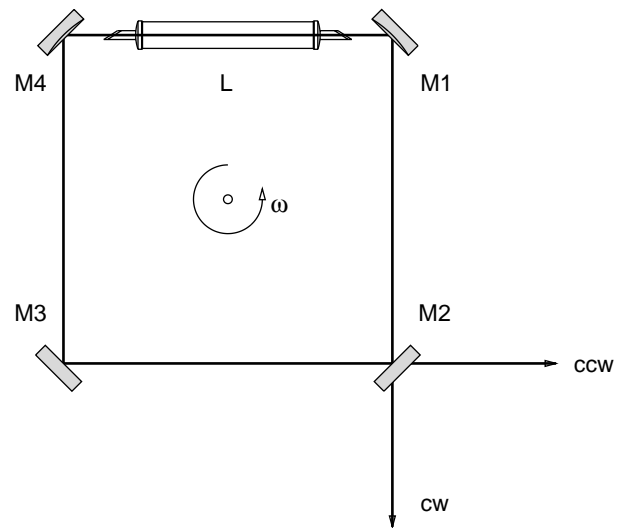


Fig. 15: Ring Laser

Here, one wave runs in the clockwise direction (cw, clock-wise) and the other in the counter clockwise direction (ccw, counter clock-wise). The mirror M2 is placed in such a way, that it permits a part of the laser beam to pass through, or in Laser Physics jargon, “decoupled”, namely ccw and cw. When both the beams are combined together again with other optical components, they produce an interference pattern on a screen. If the ring laser is now put in rotation, the pattern changes, corresponding to equation (6). Contrary to the passive optical gyroscopes used by Sagnac, the ring laser represents an active system, for whose dimensioning the optical properties of the mirror arrangement as well as the dynamic properties of the active laser material must be considered. In the next section, hence, we shall deal with the calculation and the design of the optical resonators.

2.6 ABCD Matrices

In the following section, certain basic concepts about the calculation and the description of the optical resonator will be explained. For the resonator type used in the later experiments, the optical stability criteria and the beam radius course has been calculated and discussed. The calculations have been done for an “empty” resonator, since the resonator properties can be especially influenced depending upon the active laser material (e.g. thermal lenses, abnormal refractive index etc.). In this context, the ABCD law will be introduced and used. This type of optical computation is an elegant method for ray tracing in a complex optical system. As shown in the next figure (figure 16), an equivalent lens system can be constructed for each optical resonator.

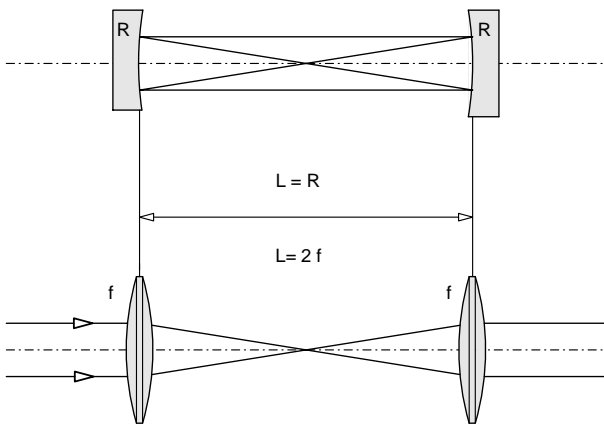


Fig. 16: Spherical resonator with equivalent lens guide

It must be noted here, that the number of gyrations would be endless in a resonator or else one can imagine a system with a number of lenses as shown in figure 16. One gets an *optically stable* resonator only when such optical imaging properties are selected, that after endless passes the ray diameter remains smaller than the mirror diameter. With the help of ABCD or the matrices on one hand the ray path of the resonator can be traced mathematically in its equivalent lens guide, and on the other a criteria can be specified for the distances L of the mirrors used, at which an optical resonator would be “stable”.

How does the ABCD law work?

First, we must assume that the following calculations for the limiting case of geometrical optics are correct. This in addition, when the angle of the rays to the optical axis is $< 15^\circ$, i.e. $\sin\alpha \approx \alpha$ at a good approximation. This condition is fulfilled for most of the systems, especially for the laser resonator. A light ray is then uniquely defined through its height x to the optical axis and the inclination at this point (Figure 17).

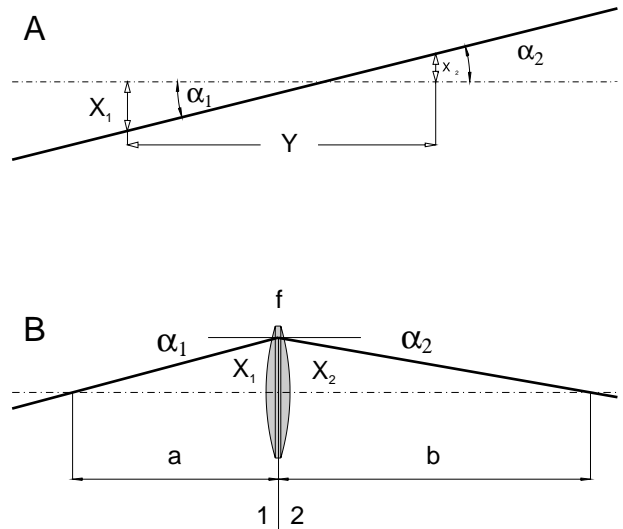


Fig. 17: Characteristic quantities for A.) Light ray B.) Thin lens

A matrix is introduced, which when applied to the initial quantities X_1 and α_1 gives the final quantities X_2 and α_2 :

$$\begin{pmatrix} X_2 \\ \alpha_2 \end{pmatrix} = \begin{pmatrix} A & B \\ C & D \end{pmatrix} \cdot \begin{pmatrix} X_1 \\ \alpha_1 \end{pmatrix}$$

The matrix thus introduced is called ray transfer matrix or the ABCD-matrix. From the example given in figure 17A of the free propagation of a ray we can see, that $\alpha_1 = \alpha_2$ and $X_2 = X_1 + Y \alpha$. The ABCD-matrix for this case will then be:

Free ray propagation $A_1 = \begin{pmatrix} 1 & Y \\ 0 & 1 \end{pmatrix}$

For the example B of a thin lens, one gets the corresponding matrix from the following:

1. Just before (1) and after (2) the lens is $X_1 = X_2$
2. The slope of the ray in area (2) is $\alpha_2 = \frac{X_2}{b}$
3. With the image equation $\frac{1}{f} = \frac{1}{a} - \frac{1}{b}$ and $a = \frac{X_1}{\alpha_1}$

One thus gets the ABCD-matrix for a thin lens: $A_2 = \begin{pmatrix} 1 & 0 \\ -\frac{1}{f} & 1 \end{pmatrix}$

With this method one can imagine a whole series of ABCD-matrices for different optical elements. However, the above examples suffice fully for the calculation of a resonator.

One can now see, that the combination of example A and B, free ray propagation with subsequent passage through a thin lens occurs as a result of arranging systems A and B one after the other.

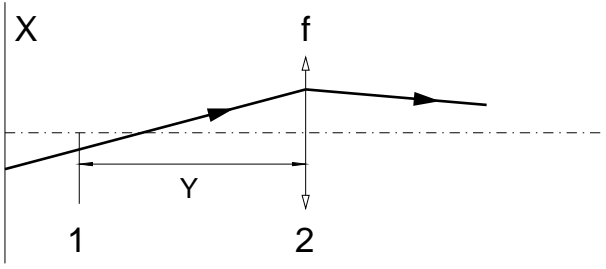


Fig. 18: Passage through a thin lens

At point 1 the ray has the coordinate X_1 and the slope α_1 and in the distance Y from the lens of the focus f (point 2) the desired values are X_2 and α_2 .

By applying the ABCD-matrix for the free ray propagation (A_1) and of the thin lens (A_2) on the initial coordinates, we get:

$$\begin{pmatrix} X_2 \\ \alpha_2 \end{pmatrix} = A_2 \cdot A_1 \cdot \begin{pmatrix} X_1 \\ \alpha_1 \end{pmatrix}$$

$$\begin{pmatrix} X_2 \\ \alpha_2 \end{pmatrix} = \begin{pmatrix} 1 & 0 \\ -\frac{1}{f} & 1 \end{pmatrix} \cdot \begin{pmatrix} 1 & Y \\ 0 & 1 \end{pmatrix} \cdot \begin{pmatrix} X_1 \\ \alpha_1 \end{pmatrix}$$

$$\begin{pmatrix} X_2 \\ \alpha_2 \end{pmatrix} = \begin{pmatrix} 1 & Y \\ -\frac{1}{f} & 1 - \frac{Y}{f} \end{pmatrix} \cdot \begin{pmatrix} X_1 \\ \alpha_1 \end{pmatrix}$$

In the meantime, we keep the ABCD matrix A_3 fixed, which then describes the path of the ray through a thin lens:

$$A_3 = \begin{pmatrix} 1 & Y \\ -\frac{1}{f} & 1 - \frac{Y}{f} \end{pmatrix}$$

Finally, we get the following as the result:

$$\begin{pmatrix} X_2 \\ \alpha_2 \end{pmatrix} = \begin{pmatrix} X_1 + \alpha_1 Y \\ -\frac{1}{f} X_1 + \alpha_1 \left(1 - \frac{Y}{f}\right) \end{pmatrix}$$

With these concepts, we are now ready to calculate a lens guide, in order to specify the optical stability criteria of a laser resonator with this knowledge. As already mentioned, the light rays travel infinitely back and forth in an optical resonator. In the case of the equivalent lens guide this implies, that the same optical structure is traversed infinite times. After n passages, the ABCD law becomes the following for any specific place of the lens guide (figure 16):

$$\begin{pmatrix} X \\ \alpha \end{pmatrix}^n = \begin{pmatrix} A & B \\ C & D \end{pmatrix}^n \begin{pmatrix} X \\ \alpha \end{pmatrix} \quad (7)$$

The ABCD matrix thereby is the equivalent lens guide allocated to the resonator. It would now be very cumbersome to solve the above expression for a few thousand values of n . Fortunately; the n^{th} power of a 2×2 matrix can be calculated much more simply:

$$\begin{pmatrix} A & B \\ C & D \end{pmatrix}^n = \frac{1}{\sin(\theta)} \begin{pmatrix} A \sin(n\theta) - \sin((n-1)\theta) & B \sin(n\theta) \\ C \sin(n\theta) & D \sin(n\theta) - \sin((n-1)\theta) \end{pmatrix}$$

Here $\theta = \arccos\left(\frac{A+D}{2}\right)$. (8)

So that the linear system of equations remains solvable, i.e. the rays after infinite passages remain within the lens guide, equation (8) demands:

$$\left| \frac{A+D}{2} \right| \leq 1 \quad (9)$$

This is now the stability criteria for the lens guide and hence also for the related resonator. Within the scope of this project, we shall be dealing with a special type of resonator, which forms the basis of the laser gyro discussed here Figure 19.

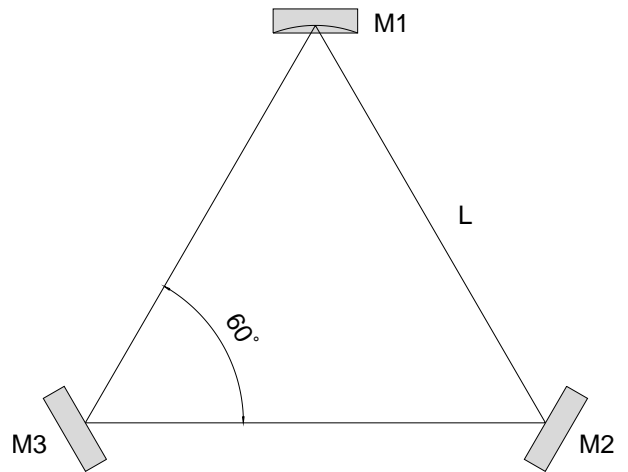


Fig. 19: Ring resonator with three mirrors

For convincing reasons, which we shall mention later on, a symmetric three-mirrored ring resonator is used for the laser gyro. The mirror M1 has a radius of curvature R , whereas the mirrors M2 and M3 are flat mirrors. The equivalent lens guide has been shown in figure 20:

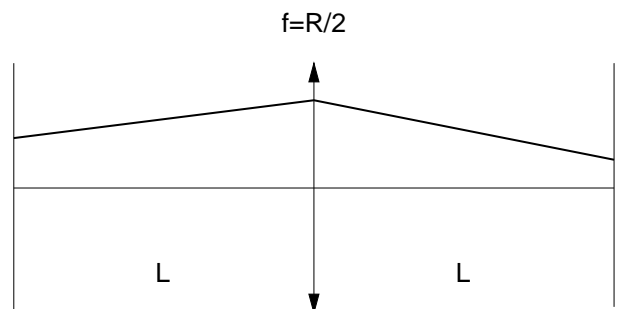


Fig. 20: Equivalent lens guide for the ring resonator as shown in figure 19

The equivalent lens guide comprises of three stages (from left to right):

- 1) Free ray path
- 2) Passage through a thin lens
- 3) Free ray path

The related matrices thus become:

$$A = \begin{pmatrix} 1 & L \\ 0 & 1 \end{pmatrix} \cdot \begin{pmatrix} 1 & 0 \\ -\frac{1}{f} & 1 \end{pmatrix} \cdot \begin{pmatrix} 1 & L \\ 0 & 1 \end{pmatrix}$$

$$A = \begin{pmatrix} 1 & L \\ 0 & 1 \end{pmatrix} \cdot \begin{pmatrix} 1 & L \\ -\frac{1}{f} & 1 - \frac{L}{f} \end{pmatrix}$$

$$A = \begin{pmatrix} 1 - \frac{L}{f} & L + L(1 - \frac{L}{f}) \\ -\frac{1}{f} & 1 - \frac{L}{f} \end{pmatrix}$$

With equation (9) one gets the stability criteria for this arrangement as:

$$\frac{|A+D|}{2} = \left| 1 - \frac{L}{f} \right| = \left| 1 - \frac{2L}{R} \right| \leq 1 \quad (10)$$

Apparently, the resonator is optically stable, when the distance L fulfils the following condition:

$$\frac{R}{2} \leq L \leq R \quad (11)$$

For dimensioning the resonator as laser gyro, a best possible compromise must be made considering on one hand the desired area A encompassed by the ray and on the other the active laser material.

2.7 Helium Neon Laser

2.7.1 He-Ne energy- level diagram

The fascination for inert gases and their clear atomistic structure formed the basis for many spectroscopic investigations. The knowledge obtained through spectroscopic data was extremely helpful in deciding to choose helium and neon for the first lasers, using Schawlow Towne's discovery of lasing conditions in 1958 to estimate whether an inversion was feasible in laser operation. The lifetime of the s- and p-states were well known. Those of the s-states were longer than those of the p-states by a factor of about 10. The inversion condition was therefore fulfilled.

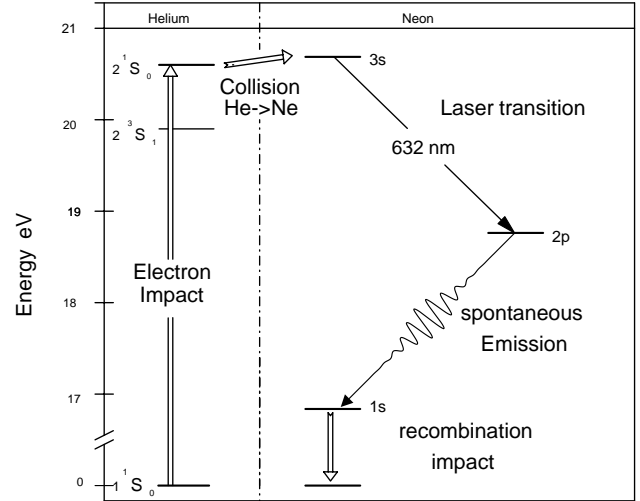


Fig. 21: Excitation and Laser process for the visible Laser emission

Fig. 21 shows the reduced energy-level diagram for helium and neon. Only those levels important in the discussion of the excitation and laser processes at a wavelength of 632 nm are indicated.

The left side of the representation shows the lower levels of the helium atoms. Note that the energy scale is split and that there is a larger difference in energy in the recombination process than is evident in the diagram. Paschen's names for the neon energy levels are used (Racah's term descriptions are often found as well). The terms are simply numbered consecutively, from bottom to top. A characteristic of helium is that its first states to be excited, 2^1S_1 and 2^1S_0 are metastable, i.e. optical transitions to the ground state 1^1S_0 are not allowed, because this would violate the selection rules for optical transitions. Because of the gas discharge, these states are populated by electron collisions (collision of the second type, Fig. 22).

A collision is called a collision of the second type if one of the colliding bodies transfers energy to the other so that a transition from the previous energy state to the next higher or lower takes place. Apart from the electron collision of the second type there is also the atomic collision of the second type. In the latter, an excited helium atom reaches the initial state because its energy has been used in the excitation of a Ne atom. Both these processes form the basis for the production of a population inversion in the Ne system.

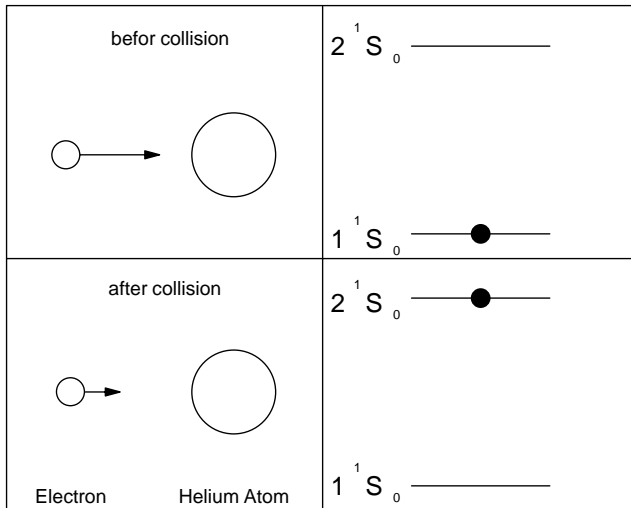


Fig. 22: Electron collision of the second kind

If we look at Fig. 21 we can see that the 2¹S₀ is slightly below the 3s level of the neon. However, the additional thermal energy kT is sufficient to overcome this gap. As already mentioned, the lifetime of the s-states of the neon are approximately 10 times longer as those of the p-states. An immediate population inversion between the 3s and the 2p levels will therefore be generated. The 2s level is emptied due to spontaneous emission into the 1s level. After this the neon atoms reaching their ground state again, primarily through collisions with the tube wall (capillary), since an optical transition is not allowed. This calming down process is the bottleneck in the laser cycle. It is therefore advisable to choose a capillary diameter that is as small as possible. However, the laser will then suffer more losses. Modern He-Ne lasers work at an optimum of these contradictory conditions. This is the main reason for the comparatively low output of He-Ne lasers.

We have discussed the laser cycle of the commonly known red line at 632 nm up to this point. However, the neon has several other transitions, used to produce about 200 laser lines in the laboratories. However, these lines do not play an important role for the technical interferometry

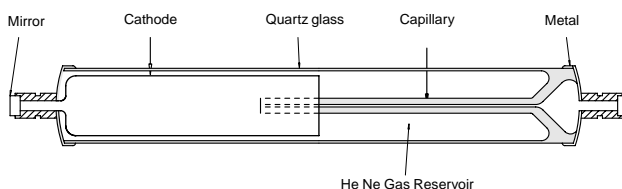


Fig. 23: Modern He Ne Laser with metal to glass soldering of the anode and cathode as well as the laser mirrors

Fig. 23 shows a modern laser tube made with highly perfected manufacturing techniques and optimised to suit the physical aspects of the laser. This applies to the resonator in particular, which is designed for a best possible output in the fundamental mode with a purely Gaussian beam and spectral purity in single mode operation (e.g. for interferometric length measurement or

laser gyroscopes). The fulfilment of this demand depends, amongst other aspects, on the optimal adaptation of the resonator to the amplification profile of the Neon. The behaviour of Neon during amplification will therefore be discussed first.

2.7.2 Gain Profile of Neon

The Neon atoms move more or less freely in the laser tube but at different speeds. The number N of neon atoms with the mass m, within a speed interval of v to v+dv is described according to the Maxwell-Boltzmann distribution (Fig. 5).

$$\frac{n(v)}{N} = \frac{4}{\sqrt{\pi}} \cdot \frac{v^2}{\sqrt{(2kT/m)^2}} \cdot e^{-\frac{mv^2}{kT}} dv$$

T is the absolute temperature and k Boltzman's constant and the above equation is applicable for all directions in space. However, we are only interested in the distribution of speed in the direction of the capillary. Using v² = v_x² + v_y² + v_z² we obtain for the direction x:

$$\frac{n(v_x)}{N} = \sqrt{2kT/m} \cdot e^{-\frac{m \cdot v_x^2}{kT}} dv_x \tag{12}$$

A resting observer will now see the absorption or emission frequency shifted, due to Doppler's effect (Ch.Doppler: Abh. d. K. Boehmischen Ges.d.Wiss. (5). Vol.II (1842) P.465), and the value of the shift will be:

$$v = \frac{v_0}{1 \pm v/c} \text{ Assuming } v \ll c \tag{13}$$

v₀ is the absorption or emission frequency of the resting neon atom and c the speed of light. If the Doppler equation (12) is used to substitute the velocity v in the Maxwell-Boltzmann's velocity distribution (13) the line broadening produced by the movement of Neon atoms can be found. Since the intensity is proportional to the number of absorbing or emitting Neon atoms, the intensity distribution will be:

$$I(v) = I(v_0) \cdot e^{-\left(\frac{c \cdot v - v_0}{v_0 \cdot v_w}\right)^2} \tag{14}$$

v_w is the most likely speed according to: $v_w = \sqrt{\frac{2kT}{m}}$

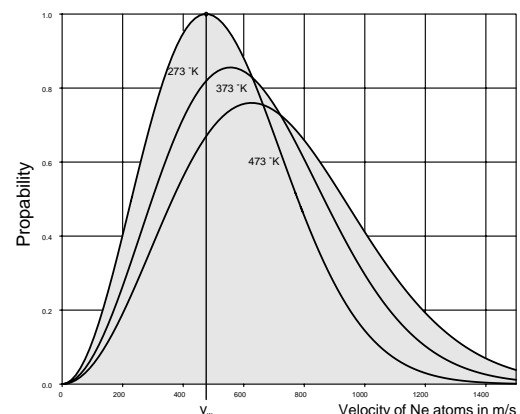


Fig. 24: Probability Distribution for the velocity v of the neon atoms at an interval v to $v + dv$.

The full width at half maximum is calculated by setting $I(v)=1/2 I(v_0)$ and the result is:

$$\Delta v_{\text{Doppler}} = \sqrt{4 \cdot \ln 2} \cdot \frac{v_w}{c} \cdot v_0 \quad \text{Eq. 2.1}$$

We can conclude from Eq. 2.4 that the line broadening caused by Doppler's effect is larger in the case of:

- Higher resonance frequencies v_0
- Or smaller wavelengths ($v_0=c/\lambda_0$, UV-lines)
- Higher most likely velocity v_w
- That means higher temperature T

and smaller in the case of:

- A larger particle mass.

The line profile also corresponds to a Gaussian distribution curve (14). Fig. 26 shows this kind of profile. The histogram only approaches the distribution curve when the speed intervals dv are small.

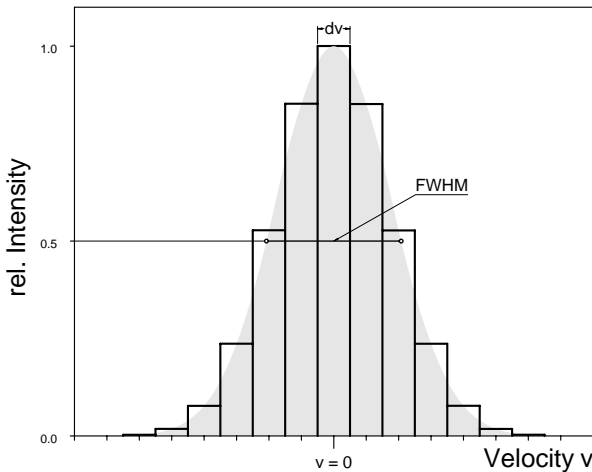


Fig. 25: Inhomogeneous line profile, speed intervals dv

On closer observation, we can see that a line broadened by the Doppler effect actually does not have a pure Gaussian distribution curve. To understand this, we pick out an ensemble of Ne atoms whose speed components have the value v in the direction we are looking at. We expect that all these atoms emit light with the same frequency v

$$v = v_0 \left(1 \pm \frac{v}{c}\right)$$

However, we have to consider an additional effect, which is responsible for the lifetime of a transition.

$$\tau_s = \frac{1}{A_{ik}}$$

The exact profile formation can be determined from the convolution of the Gaussian profile with the individual Lorentz profiles. The result obtained in this manner is called as the Voigt profile.

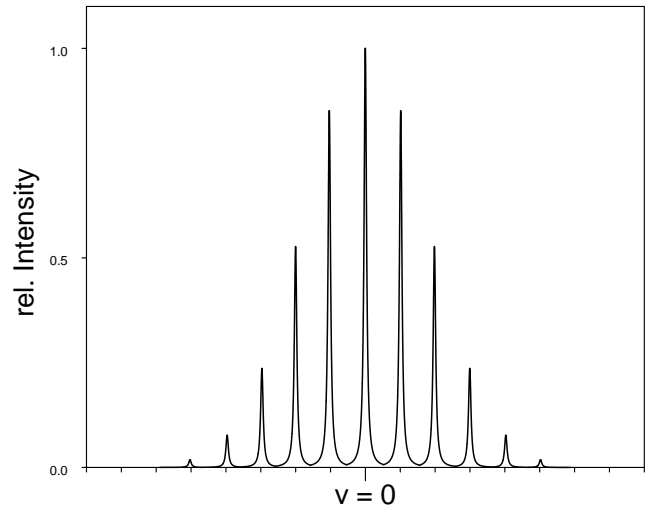


Fig. 26: Natural broadened line profiles (homogeneous) for groups of speed v within the inhomogeneous Doppler broadened gain profile

Equivalent to the cavity resonator the Laser resonator shows oscillation modes, which have to fulfil the condition:

$$L = n \cdot \frac{\lambda}{2} \quad (15)$$

or

$$L = n \cdot \frac{c}{2v},$$

L represents the length of the resonator, λ the wavelength; c the speed of light, v the frequency of the generated light and n is an integer number. Thus, every mode has its frequency of

$$v(n) = n \cdot \frac{c}{2L}$$

e.g. A He-Ne-Laser with a resonator length of 30 cm at an emission wavelength λ of 632.8 nm will have the following value for n :

$$n = \frac{v}{c} \cdot 2 \cdot L = 2 \cdot \frac{L}{\lambda} = 2 \cdot \frac{0,3}{632,8 \cdot 10^{-8}} = 949.167$$

The difference in frequency of two neighboured modes is:

$$\Delta v = v(n+1) - v(n) = (n+1) \cdot \frac{c}{2L} - n \cdot \frac{c}{2L} = \frac{c}{2L}$$

$$\text{or } \Delta v = \frac{c}{2d} \quad (16)$$

In the above example the distance between modes would be

$$\Delta v = \frac{3 \cdot 10^8}{2 \cdot 0,3} = 5 \cdot 10^8 \text{ Hz} = 500 \text{ MHz}$$

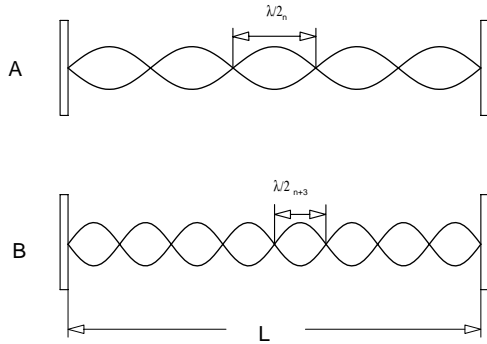


Fig. 27: Standing longitudinal waves in an optical resonator. A with n nodes and B with n+3 nodes

If the active laser material is now brought into the resonator standing waves will be formed due to the continuous emission of the active material in the resonator and energy will be extracted from the material. However, the resonator can only extract energy for which it is resonant. In contradiction to the empty resonator where L is the mechanical length for the “filled” resonator the index of refraction of the filling has to be taken into account as:

$$L = n_{ior} \cdot L_{AM} + L_e \quad (17)$$

Whereby L_e represents the length of the empty resonator and L_{AM} the length of the filled zone having the index of refraction n_{ior} . In principle, a resonator has an indefinite number of modes, whereas the active material only emits in an area of frequency determined by the emission line width. Fig. 28 shows the situation in the case of material that is inhomogeneously broadened.

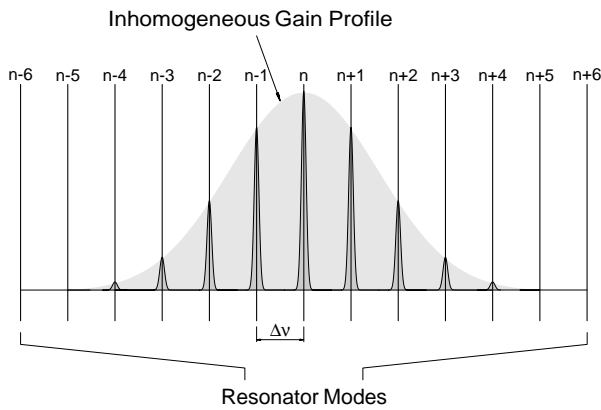


Fig. 28: Inhomogeneous emission profile in interacting with an optical Resonator

If the laser is operating in a stationary state, we can see that it is emitting several longitudinal modes. These are exactly the same modes that will be found in the emission profile. Since the modes are fed by an inhomogeneous emission profile, they can also exist independently. Now one could assume that it will be very difficult to keep the length of the resonator exactly matching the resonance condition of (15) and (17). Therefore, it should be noted that near the resonance of a transition the index of refraction strongly depends on the detuning from resonance and thus allowing a mode to oscillate on another fre-

quency as it would in an empty resonator. This effect is also termed as „frequency pulling and pushing“.

2.8 Modes of the ring resonator

In the case of a resonator with two mirrors, as for example in figure 29, a standing wave arises because of the fact that the waves travelling forward (f) and backward (b) overlap each other. When we apply this picture to a ring resonator, the wave travelling forward (f) becomes the one passing through the resonator in the clockwise direction (cw, “clock-wise”), and the wave travelling backward becomes the one going in the counter clockwise direction (ccw, “counter clock-wise”).

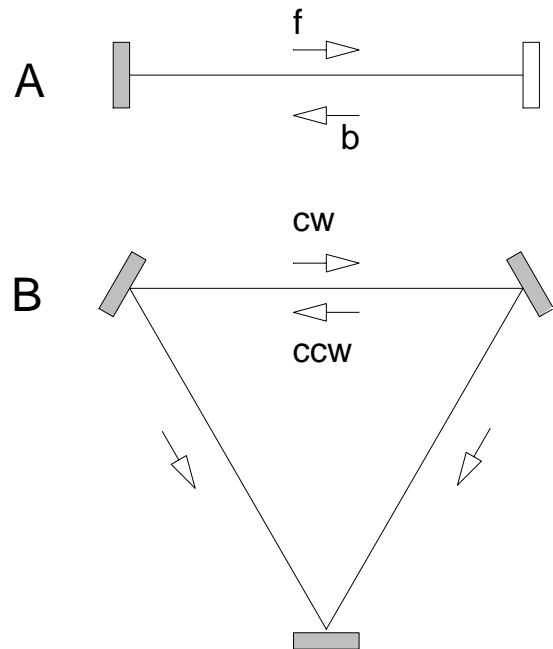


Fig. 29: Linear (A) and Ring resonator (B)

For the ring laser it is essential, that a multiple of the complete wavelength must “fit” in the resonator. If this is not the case, the gyrating wave will interfere with itself destructively and the desired laser oscillation will not be generated. The following applies to the ring laser as an amendment to equation (16) that defines the frequency difference of two longitudinal modes of the standing wave resonator:

$$\Delta\nu = \frac{c}{L}$$

Note that L here stands for the complete resonator length.

As is already known for the standing wave resonator, in which the waves travelling forward and backward are fed from different speed classes, this is also the case for the ring laser for the cw and the ccw mode (figure 30):

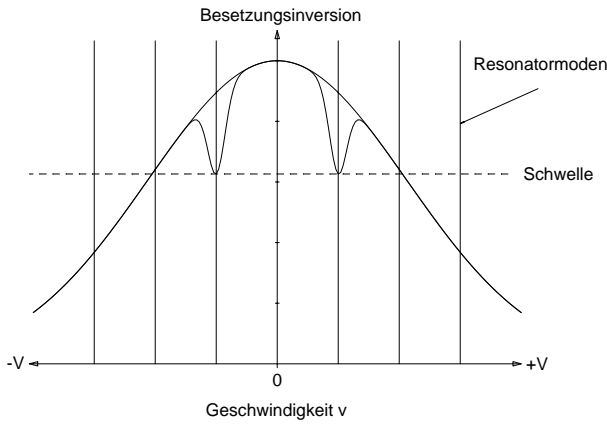


Fig. 30: Both the modes of the ring resonator are fed from different classes of velocity

In the example shown in figure 29 one can expect, that the ring laser has two modes (cw and ccw), but only one mode per direction. However, more than one mode is also possible per direction depending upon the level of the threshold. On one hand, this depends on the length of the resonator used or the specified free spectral range and the amplification (threshold). Now since the amplification again depends on the length of the HeNe discharge tube used, one selects a suitable length for the laser gyro, in order to get longitudinal one-mode oscillations per direction. Laser gyros of today are constructed in such a way, that the resonator and the discharge path form a compact block. Hence, as a "black box", they are not very suitable for didactic purposes. However, an open system will be used within this project containing a laser tube sealed with a Brewster window. In the models available, the active length is such that the ring laser shows longitudinal multi-mode oscillations. A selective element is used for getting the necessary one-mode oscillations. This selective element brings the ring laser in the required operational state.

2.9 Mode selection

With a so-called Etalon, it is possible to cause frequency-selective losses in the resonator, so that the undesired modes can be damped and suppressed. An Etalon is a parallel resonator having a lower quality. Most of the times the etalon comprises of a single glass body, whose plane surfaces are very well ground and polished parallel to each other. Like a normal resonator, the etalon also has modes. However, the modes are essentially broader, since the reflection of the plane surfaces is kept low (figure 31). The effective amplification results from the transmission curve of the etalon and the amplification of the laser active material.

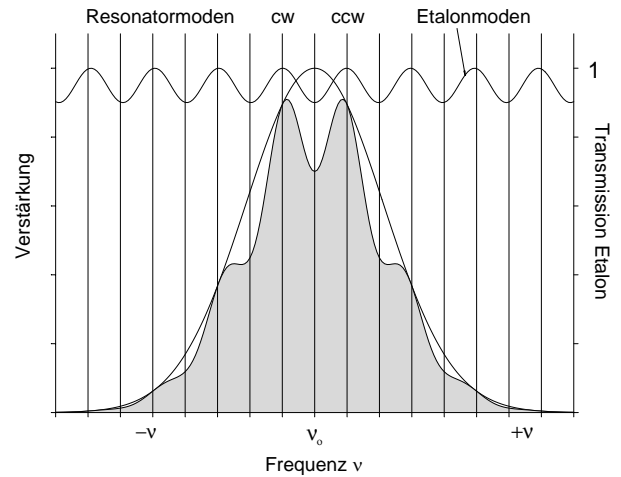


Fig. 31: Mode selection mode with an Etalon

If one tilts the etalon by an angle γ against the incident ray, the maximum of the transmission also changes accordingly:

$$v_m (T = 1) = \frac{c}{2d} \cdot m \cdot \sqrt{n^2 - \sin^2(\gamma)}$$

Here m is an integer (the order), d the thickness, n the refractive index and γ the tilt angle of the etalon. As per figure 30, the modes of the etalon can also be shifted by tilting it, where the gain profile and the resonator modes remain fixed. In this way, it is possible to cause higher losses in the modes, which could oscillate because of the change in the threshold value, than for the modes, which are just below the maximum value of transmission for the etalon. Figure 30 shows two modes, cw and ccw. Both the modes have a mutual frequency difference corresponding to equation (16). If one tilts the etalon, one gets the situation as shown in figure 32. In this case, both the cw and ccw waves possess the same frequency, which is of an advantage to the laser gyro.

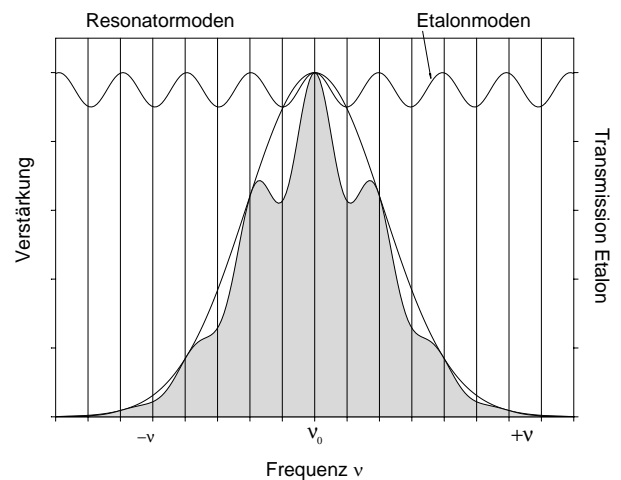


Fig. 32: Etalon tuned to resonance, the cw and the ccw waves have the same frequency

Depending on how strongly the undesired modes have to be suppressed, and the spectral distance, which they have, the appropriate thickness d of the etalon must be

selected. In case of the HeNe ring laser of the following experiments, the etalon is 1 cm thick and does not have any additional mirror coating, but instead only 4% reflection due to Fresnel reflection.

2.10 Transverse modes

For the sake of simplicity, the laser and resonator properties were discussed for an example of a plane parallel resonator. In practice, this type of resonator is not used due to its disadvantageous characteristics.

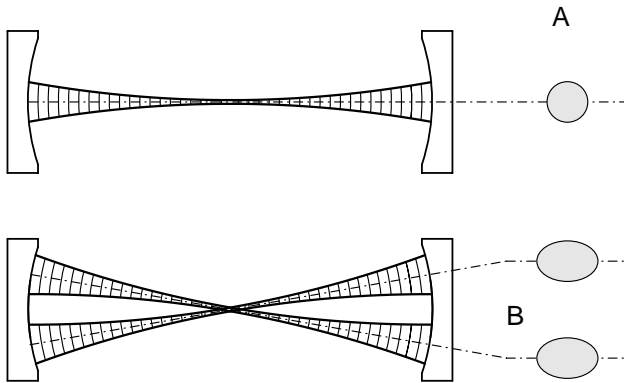


Fig. 33: A spherical resonator with oscillation in the fundamental TEM_{00q} (A) and a transverse mode TEM_{01q} (B)

The hemispherical resonator has become very popular, since it exploits in a special manner the desired mode characteristics of the plane parallel resonator and the advantages of adjustment associated with the spherical resonator. However, a disadvantage accompanies this advantage. Whereas almost exclusively longitudinal modes excite in the plane parallel resonator, transversal modes can also arise in spherical resonators. This effect is shown in Fig. 33. When the laser operates in the steady state, the wave fronts at the mirrors have the same radius of curvature as the mirrors themselves. The situation is drawn in case A in which a radiation field has formed symmetrically about the optical axis. At the resonator output, one can see a round Gaussian shaped intensity distribution. However, it is also possible for a radiation field to be set up at an angle to the resonator's optical axis. In principle a multitude of this type of radiation field can develop, because in all of these cases the radius of curvature for the radiation field at the mirrors is the same as that of the mirrors. At the resonator output, one can now observe intensity distributions spatially separated and no longer symmetrical about the axis of radiation. Since these modes do not oscillate in the direction of the optical axis (longitudinal) but are mainly transversal, these modes are termed transversal modes. Owing to the large number of modes, a convention has been adopted in which the relevant modes are given a universal designation:

$$T E M_{m n q}$$

TEM stands for **T**ransverse **E**lectromagnetic **M**odes. The indices m, n and q are integer numbers, which state the number of intensity spots minus one in the X axis (m)

and the number in the Y axis (n), which are observed. The basis for this consideration is the fundamental mode TEM_{00q} that produces just a round spot. In the example of fig. 33 (B) the designation is:

$$T E M_{01q}$$

The number q states how many nodal points the standing wave in the resonator has. This number does not have any significance for the user of the laser and is therefore generally omitted.

It can easily understand that for the laser gyroscope measures has to be taken to avoid the occurrence of such modes. In the simplest case, a pinhole placed at a particular location inside the resonator (fig. 34) is used. The diameter of the pinhole is chosen so that the transverse modes are suppressed whereas the longitudinal modes can pass it without hindrance.

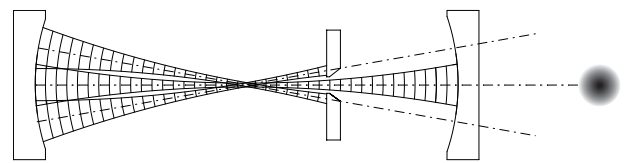


Fig. 34: Suppression of transverse modes by means of a pinhole

Since laser rays are Gaussian rays the beam diameter is not constant and varies from the distance to its beam waist. A Gaussian beam always has a waist. The beam radius w results out of the wave equation as follows:

$$w(z) = w_0 \cdot \sqrt{1 + \left(\frac{z}{z_R}\right)^2}$$

w₀ is the smallest beam radius at the waist and z_r is the Rayleigh length

$$z_R = w_0^2 \frac{\pi}{\lambda}$$

In Fig.: 35 the course of the beam diameter as a function of z is represented. The beam propagates within the direction of z. At the position z = z₀ the beam has the smallest radius.

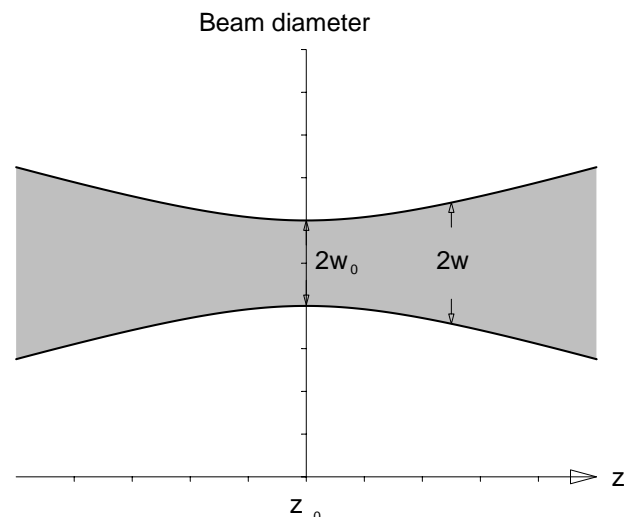


Fig. 35: Beam diameter of a Gaussian TEM₀₀ beam versus the location z

As also shown in figure 34, it is useful to keep the pin hole as near to the beam waist as possible, because if the distance is more, the transverse modes would overlap significantly with the fundamental mode, so that the pin hole would weaken the fundamental mode. Since we will be working with a commercial HeNe laser tube in this project, we get the pinhole in the form of an in-built capillary. We now only have to select the geometry of the ring resonator in such a way, that the position of the beam waist is in the capillary (figure 35). If the length L is given, the radius of curvature must be selected accordingly to fulfil this condition

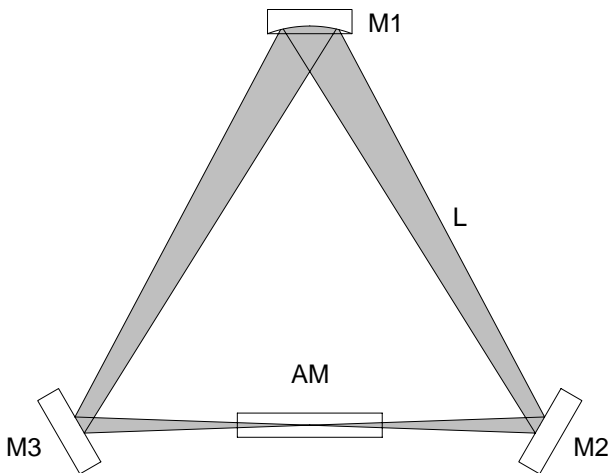


Fig. 36: Geometric path of the ray, when the radius of curvature of the mirror is R=3L

Finally, it must be checked, whether this arrangement is also optically stable. For this, we use the stability criteria as per (10):

$$\left| 1 - \frac{2L}{R} \right| \leq 1$$

and find for R=3L:

$$\left| 1 - \frac{2}{3} \right| \leq 1$$

and notice that we are not at the verge of optical stability for this value, which is :

1. R= 2L
2. R= 4L

In the given case, that one is at the border of the optical stability, there is a risk of thermal drift, because of which the resonator can change over to the unstable state and therefore not produce any more laser oscillations.

2.11 The Laser gyro

We now have collected the required knowledge for operating a transverse and longitudinal single-mode Helium-Neon laser gyro. In this section we shall discuss what happens to the laser modes, when this ring laser is set in rotation. To analyse the modes, we must decouple a part

of the radiation of the resonator. For this purpose, one of the mirrors is provided with a low transmission.

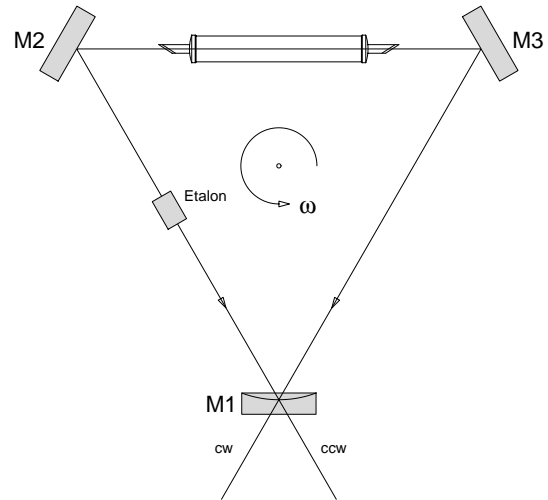


Fig. 37: Laser gyro with three mirrors, decoupling of the modes at the mirror M1

There are different models for describing the effect of the rotation on the ring laser. We shall select a clear way with the help of the Doppler effect. In section 2.7.2, we have already learnt the fundamentals. The starting point of the laser oscillations is the spontaneous emission, produced by the excited neon atoms. When such an atom is at rest, it emits the frequency ν_0 . If it now starts moving at velocity v, this frequency changes because of the Doppler effect to:

$$\nu = \nu_0 \left(1 + \frac{v}{c} \right)$$

If the velocity has been produced as a result of the rotation, one gets the following value for v:

$$v_{rot} = r \cdot \omega$$

where ω is the angular speed and r is the distance of the atom to the centre of rotation. As a result of the rotation, the emissions frequency changes to:

$$\nu_+ = \nu_0 \left(1 + \frac{v}{c} + \frac{r \cdot \omega}{c} \right)$$

The above expression applies to atoms, whose velocity v is in the direction of rotation. The following expression applies to atoms, whose velocity is against the direction of rotation:

$$\nu_- = \nu_0 \left(1 - \frac{v}{c} - \frac{r \cdot \omega}{c} \right)$$

The difference $\Delta\nu$ of both the frequencies thus becomes:

$$\Delta\nu = \nu_+ - \nu_- = \nu_0 \left(\frac{v}{c} + \frac{2 \cdot r \cdot \omega}{c} \right)$$

The portion caused only by rotation has the value:

$$\Delta v_{\text{rot}} = v_0 \frac{2 \cdot r \cdot \omega}{c} = \frac{4 \cdot F}{L \cdot \lambda} \cdot \omega \quad (18)$$

Here, we substitute:

$$F = \pi \cdot r^2 \text{ und } L = 2 \cdot \pi \cdot r$$

and get the same expression as for the Sagnac effect with passive resonator.

2.11.1 Lock-in Effect

However, there is one restriction for equation (18) for the actual operation of a ring laser. Below a certain rate of rotation, no differential frequency occurs i.e. both the modes do not change their frequencies. Such behaviour can only be explained by a coupling of both the modes. This coupling occurs because parts of the intensity of one mode go into the other. This happens through scattered light that arises at the surfaces of the resonator mirror. Even today, it is not possible to produce laser mirrors that do not show any scattering. In practice, this leads to an effect, which poses a certain restriction to the working of the laser gyro. The scattered light, appearing unavoidably at the mirrors, leads to an "impurity" of the cw mode with few parts of the ccw mode and vice versa. Hence, both the modes couple, since they are affected by the scattered light from the other mode. This coupling can be broken, when the rate of rotation of the gyro exceeds a certain limit. In that case, the resonance frequency of the system for both the modes is separated to such an extent, that the laser has to give up the coupling, in order to oscillate. This coupling is also called as lock-in effect and the limit, at which this coupling is broken, is called the lock-in limit. As already mentioned the cause for the lock-in effect is the scattering at the optical splitting components. When the laser beam strikes an optical surface, scattered light always appears in practice that goes in different directions of space depending upon the texture of the surface.

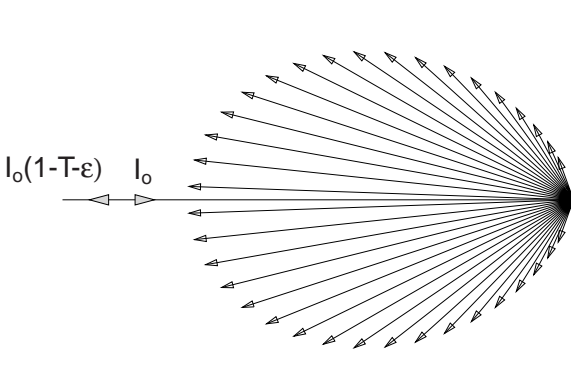


Fig. 38: Light scattering at an optical surface

When a laser beam strikes a reflecting optical surface with the intensity I_0 , the reflected ray has an intensity of only $I_0 \cdot (1 - T - \epsilon)$, whereby T is the degree of transmission and ϵ is the back scattering coefficient. Standard laser mirrors can be produced with $T \approx 1\%$

and $\epsilon \approx 10^{-4}$. Now only that scattered light will have an effect on the laser process, which is scattered in the direction of the laser mode (figure 38) and has the same phase. Although the back scattering coefficient is relatively small, it is sufficient to couple both the gyrating modes and produce the lock-in effect.

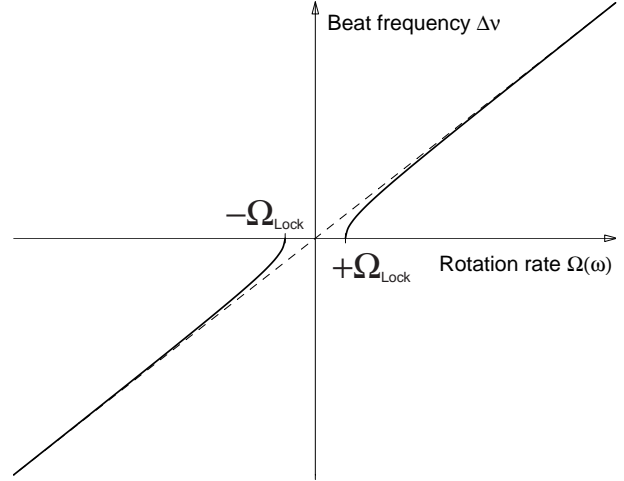


Fig. 39: Lock-in Effect

In principle, the lock-in effect can then be fully eliminated, if one can make ϵ zero. In spite of the best polishing and damping, no mirror can be produced today with $\epsilon = 10^{-7}$. The mathematical description of the lock-in effect is very complex and a complete solution is still not known, since a number of parameters are affecting the effect. For this reason, we shall be using here only the results of the model developed by Aronowitz (Fredrick Aronowitz, The Laser Gyro in "Laser Application" Vol. 1, p. 134, Academic Press 1971). According to this, there are three areas (also see figure 38) for the beat frequency between both the ring laser modes:

$$\Delta v = \begin{cases} 0 & \Omega \leq \Omega_{\text{Lock}} \\ \pm \sqrt{\Omega^2 - \Omega_{\text{Lock}}^2} & \Omega \geq \Omega_{\text{Lock}} \\ \Omega & \Omega \gg \Omega_{\text{Lock}} \end{cases}$$

Here $\Omega = \frac{8\pi F}{L\lambda} \cdot \omega$ and $\Omega_{\text{Lock}} = A \cdot \frac{c}{L}$ with A as amplitude are of a mode. There is no beat frequency below the threshold Ω_{Lock} , above it a non-linear relationship and a linear relationship only for higher values of Ω . Aronowitz gives the following equation as approximation value for the lock-in threshold:

$$\omega_{\text{Lock}} = \frac{c \cdot \lambda}{8\pi F} \cdot r \cdot \cos(\beta)$$

In the above expression r is the back scattering coefficient and β is the phase angle between the back scattered and the resonator wave. Taking the worst case, when β is just 0° , the back-scattering coefficient is about 10^{-4} and

the leg length of the ring laser is 0.5 m, we get the following value for the lock-in threshold:

$$\omega_{\text{Lock}} = \frac{3 \cdot 10^8 \cdot 632 \cdot 10^{-9}}{8 \cdot \pi \cdot 0,25 \cdot \sin(60)} \cdot 10^{-4} \approx 0,2 \text{ } ^\circ/\text{s}$$

This is a typical value for a good laser gyro. One could say here, that the lock-in effect would put a question mark over the substitution of the mechanical gyro by the laser gyro. However, this desire is so strong, that one is and always was on the lookout for ways of eliminating the lock-in threshold or at least reducing it to such an extent, that this aim could be fulfilled. The first solution naturally is to let the ring laser rotate at constant speed above the lock-in threshold. However, this reveals the practical difficulty, that the necessary electrical signals and supplies are fed to the system and taken off from it. Worldwide a procedure has been adopted which although does not eliminate the lock-in effect, but certainly reduces its effect on the measurement inaccuracy. For this purpose, the complete ring laser is subject to a periodic oscillation with ω_D (figure 40). Since, a very small amplitude is selected for this oscillation, one refers to it as "dither".

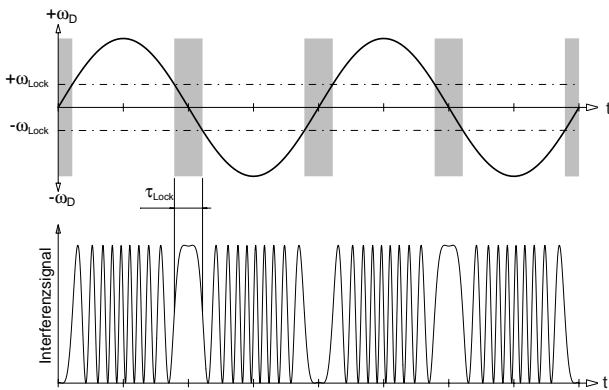


Fig. 40: The upper curve shows the angular speed of the ring laser and the lower one the interference signal.

This measure ensures that the gyro is blocked only within the time τ_{Lock} . Outside this zone, the gyro produces a certain number of light and dark bands in one as well as in the other direction, which together give the result zero. If the whole system now experiences an additional rotation, then this difference is not zero anymore, but instead gives the correct values also for the angular speeds below the lock-in threshold. However, this measurement can be falsified by the error of the blocked condition during τ_{Lock} . The error thus arising can be estimated as follows. For this we use the simple equation:

$$\frac{\omega_{\text{Lock}}}{\omega_D} = \frac{\sin\left(\omega \cdot \frac{\tau_{\text{Lock}}}{2}\right)}{\sin\left(\omega \cdot \frac{\tau}{4}\right)} \approx \omega \cdot \frac{\tau_{\text{Lock}}}{2}$$

At the time $t = \frac{\tau_{\text{Lock}}}{2}$ the function has the value ω_{Lock} and ω_D at one fourth of the total period τ . Since the lock area would run about twice within a full oscillation, one

gets the following for the blocked time of the ring resonator:

$$\tau_{\text{Lock}} = \frac{2 \cdot \omega_{\text{Lock}}}{\pi \cdot v_D \cdot \omega_D} \tag{19}$$

In the above equation v_D stands for the frequency and ω_D for the maximum rate of rotation of the dither. If one selects an arrangement with $v_D = 200\text{Hz}$, $\omega_D = 100 \text{ } ^\circ/\text{s}$ and the lock-in threshold may be at $1 \text{ } ^\circ/\text{s}$, then the blocked time would become:

$$\tau_{\text{Lock}} = \frac{2 \cdot 1}{\pi \cdot 200 \cdot 100} \approx 3.2 \cdot 10^{-5} \text{ sec.}$$

There are no angular speeds that are less than $1 \text{ } ^\circ/\text{s}$ within this relatively minor interval. One of the aims of the project is to determine the inaccuracy of the measurement considering the real gyro parameters present. The next section will deal with the determination and the evaluation of the gyro signals.

2.12 Measuring of the beat frequency

We could determine that the emission frequencies of the excited neon atoms changed because of the rotation. This implies, that the gain curve of the corresponding speed class also changes and hence the frequency of the related laser emission. Hence, we expect a frequency difference as per equation (18) between the cw and the ccw waves upon rotation of the system in our ring laser. There are two methods for measuring this frequency difference. The first one uses the spatial interference as already explained in the Sagnac interferometer, and the second works according to the principle of beam analysis. The advantage of this method is that it is not necessary to combine both the rays by making use of sophisticated devices, in order to produce a spatial interference.

2.12.1 Interference

Nevertheless, we shall explain the first method, since it is widely used in technical laser gyros. After this, we shall explain the ray analysis.

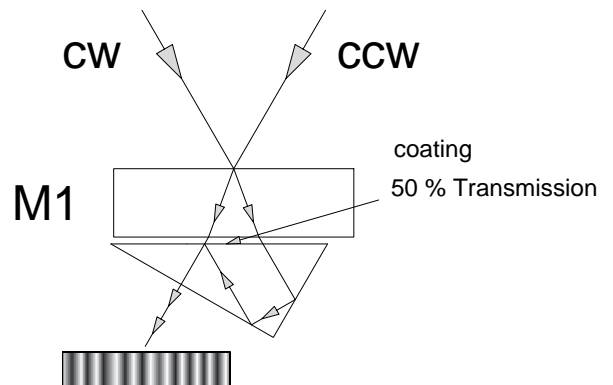


Fig. 41: Reflection prism for unifying the cw and the ccw wave

By means of a reflection prism, whose hypotenuse is coated with a translucent mirror layer (transmission 50%),

50%), the cw and the ccw waves are collated. This produces a spatial interference pattern whose light and dark transitions is detected with a photo detector and is counted. If one uses two detectors at a distance of a "half" transition (90° phase-displacement), one can determine the direction in which the gyro is rotating. The beam analysis, as shown in figure 42, has less optical effort, but the determination of the direction of rotation is more complicated here.

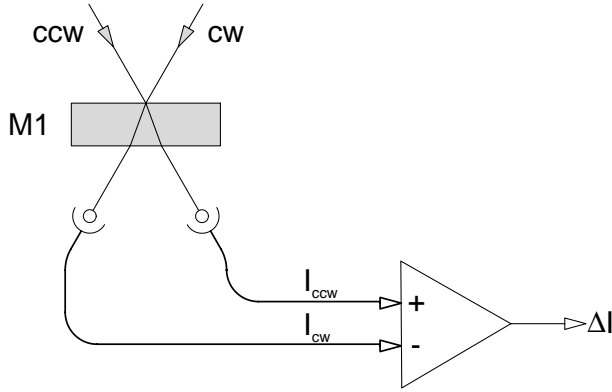


Fig. 42: Beam analysis procedure

2.12.2 Beam analysis

With this method, the intensity of the cw and the ccw waves is determined with the help of two photodetectors. One gets the desired information by subtracting both the signals. As already mentioned this process works only when a certain degree of scattering exists between the cw and the ccw waves. In reality, this is always the case. Assuming that the amplitude is A_0 in the cw as also in the ccw, then an additional wave would arise due to back-scattering, whose amplitude can be designated as $r \cdot A_0$, whereby r is the back-scattering coefficient. Now since both the waves are propagating e.g. in the cw direction, they will overlap according to the principle of superposition to form a wave with an amplitude of A_{cw} . One finally gets the intensity I_{cw} from the square of the amplitude:

$$\begin{aligned} A_{cw} &= A_0 \cdot \sin(\omega_{cw} t) + rA_0 \cdot \sin(\omega_{ccw} t + \beta) \\ &= A_0 \cdot (\sin(\omega_{cw} t) + r \sin(\omega_{ccw} t + \beta)) \\ I_{cw} &= (A_{cw})^2 \\ &= I_0 \cdot (\sin(\omega_{cw} t) + r \sin(\omega_{ccw} t + \beta))^2 \\ &= I_0 \left(\sin^2(\omega_{cw} t) + 2r \sin(\omega_{cw} t) \sin(\omega_{ccw} t + \beta) \right. \\ &\quad \left. + r^2 \sin^2(\omega_{ccw} t + \beta) \right) \end{aligned}$$

The fastest photodetectors of today are in a position to detect frequencies up to $2 \cdot 10^9$ Hz. A detector will therefore detect only the average values. The \sin^2 terms oscillate with an essentially higher frequency ω_{cw} or ω_{ccw} ,

whereby their amplitudes vary periodically between 0 and 1, so that their temporal average value is $\frac{1}{2}$.

$$I_{cw} = \frac{I_0}{2} (1 + 4r \sin(\omega_{cw} t) \sin(\omega_{ccw} t + \beta) + r^2)$$

We shall use the addition theorem for simplifying the mixed element:

$$2 \cdot \sin \alpha \cdot \sin \beta = \cos(\alpha - \beta) + \cos(\alpha + \beta)$$

The \cos term oscillates with the frequency $\omega_{cw} + \omega_{ccw}$ and its amplitude varies between -1 and $+1$, so that the average value is zero. We thus, get the following for the intensity:

$$I_{cw} = \frac{I_0}{2} (1 + 2r \cos((\omega_{cw} - \omega_{ccw})t - \beta) + r^2)$$

$$I_{cw} = \frac{I_0}{2} (1 + 2r \cos(\Delta\omega \cdot t - \beta) + r^2)$$

Moreover, for the wave running opposite, we get:

$$I_{ccw} = \frac{I_0}{2} (1 + 2r \cos(\Delta\omega \cdot t + \beta) + r^2)$$

Upon building the difference:

$$\Delta I = I_0 \cdot r \cdot (\cos(\Delta\omega \cdot t - \beta) - \cos(\Delta\omega \cdot t + \beta))$$

$$\Delta I = 2 \cdot I_0 \cdot r \cdot \sin(\Delta\omega \cdot t) \cdot \sin(\beta) \quad (19)$$

In case of the rotation of the ring laser above the lock-in threshold, equation (18) varies continuously between ΔI and $-\Delta I$ corresponding to:

$$\Delta I = 2 \cdot I_0 \cdot r \cdot \sin(\beta) \begin{cases} 1 & \Delta\omega \cdot t = n \cdot \frac{\pi}{2} \\ -1 & \Delta\omega \cdot t = n \cdot \frac{3}{2} \pi \end{cases}$$

The maximum difference of the intensities of both the modes thus becomes:

$$\Delta I_{\max} = 4 \cdot I_0 \cdot r \cdot \sin(\beta) \quad (1)$$

One would now expect that this modulation depth would be relatively small because of r . However, one must consider that the scattered wave also gains in the ring laser and thus shows a much better behaviour than expected by equation (19). In reality one gets about 30 - 40% modulation, this can be determined with the subsequent amplifying stages. Unfortunately, this method of beam analysis does not provide any information about the direction of rotation of the ring laser. This must be done by detecting the appearance of the lock-in area during the dither movement, because the direction of rotation changes precisely in this area. This can become problematic due to errors appearing in this area because of disturbances. For this reason, this procedure can be used properly only when the complete system is closed and actively stabilized. In an early developmental phase we checked in detail this process at an open system, like the one being used here, and then rejected it, since an experimental system with a lot of freedom of adjustment does not possess a fixed working point as demanded by

this process. To justify the widest possible range of possible working points, we have realized a special interference formation, which comes very close to these requirements: a push-pull interference process as shown in figure 43.

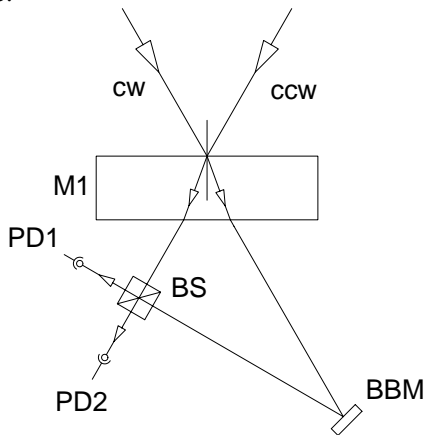
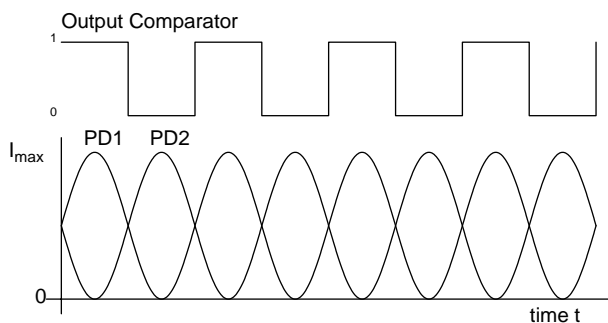


Fig. 43: Push-pull interference formation

In this arrangement, the beam splitter (BS) divides the intensity of the CCW mode in two equally large portions. The CW mode is deflected by the mirror BBM in such a way, that the beams overlap with those of the CCW modes and interfere. The interference pattern detected by the photodetector PD1 is out of phase by 180° as compared to that of PD2 (figure 44).



3 Experiments

Fig. 44: Ideal contrast

Figure 44 shows the output signals of both the photodetectors PD1 and PD2 for the unrealistic case with 100% interference contrast. A comparator switches from logical zero to one or from one to zero exactly when both the signals possess the same amplitude. It is decisive here, which of the two signals has a positive or a negative slope. We shall now consider the real case (figure 45), in which the contrast is clearly less. The advantage of using signals out of phase by 180° can be seen clearly here: the output signal of the comparator is independent of the interference contrast and offset variations in a large range.

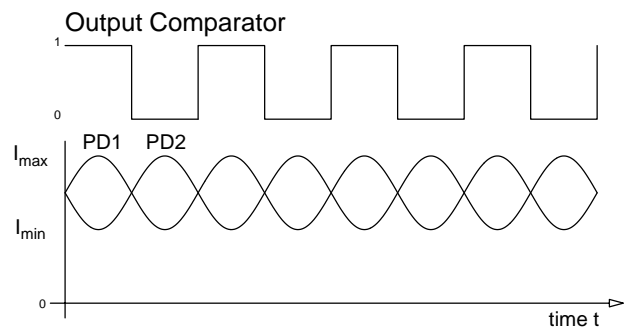


Fig. 45: Realistic contrast